Early Triassic (Induan-Olenekian) conodont biostratigraphy, global anoxia, carbon isotope excursions and environmental perturbations: New data from Western Australian Gondwana.

I. Metcalfe[1,2*], R.S. Nicoll[3], R. Willink[4], M. Ladjavadi[5], & K. Grice[5]

[1.] *Earth Sciences, Earth Studies Building C02, School of Environmental and Rural Science, University of New England, Armidale NSW 2351, Australia*

[2.] *GEMOC, ARC Centre of Excellence for Core to Crust Fluid Systems, Department of Earth and Planetary Sciences, Macquarie University, NSW 2109 Australia*

[3.] *Research School of Earth Sciences, Australian National Univ., Canberra*

[4.] *Origin Energy, Level 10, CDOP4, 135 Coronation Drive, Milton, Qld, 4064, Australia*

[5.] *WA-Organic Isotope Geochemistry Centre, Department of Chemistry, Curtin University, Perth, Australia*

* Corresponding author. Email: imetcal2@une.edu.au

Keywords: Early Triassic, Induan-Olenekian boundary, conodonts, carbon isotopes, anoxia, environmental perturbations

ABSTRACT

The Early Triassic Induan-Olenekian Stage boundary (Dienerian-Smithian Sub-Stage boundary) has been identified at a depth of 2719.25 m in the petroleum exploration well Senecio-1 located in the northern Perth Basin, Western Australia. Conodont faunas represent

three conodont zones in ascending order, the *Neospathodus dieneri* Zone, the *Neospathodus waageni eowaageni* Zone and the *Neospathodus waageni waageni* Zone. The Induan-Olenekian (Dienerian-Smithian) boundary is placed at the base of *the Neospathodus waageni eowaageni* Zone equivalent to the first appearance of *Neospathodus* ex. gr. *waageni* utilised elsewhere and adopted by the IUGS ICS Triassic Subcommission to define the base of the Olenekian. Bulk kerogen $\delta^{13}C$ carbon isotopes define a positive peak of c. 4 per mille that essentially coincides with the Induan-Olenekian boundary as seen in proposed Global Stratotype Sections and Points (GSSPs) in South China and Spiti, India demonstrating the global utility of this level for correlation. An anoxic zone is recognised in the lower part of the Senecio-1 core and the upper limit of this zone is dated as late Induan (late Dienerian). Temporal and spatial mapping of marine anoxia and dysoxia globally demonstrates that pulses of dysoxia/anoxia affected shallow-marine zones at different times in different locations. Dysoxia/anoxia in the shallow-marine environment appeared in the latest Permian at the extinction level, later than in the deep-marine environment, and appears to be largely restricted to the Induan (Griesbachian and Dienerian) and early Olenekian (Smithian). Temporally and geographically restricted upwelling of an oxygen minimum zone into the ocean surface layer due to environmental perturbations including extreme global warming, increased terrestrial chemical weathering intensity and continental erosion, sea level rise, and changes in marine nutrient inventories and productivity rates, is interpreted as a likely cause of observed variation in shallow-marine dysoxia/anoxia in the Early Triassic.

1. Introduction

The Latest Permian - Early Triassic transitional period is globally important in Earth history. It saw the most profound mass extinction known to science in the latest Changhsingian with approximately 90+ % of skeletonized marine species (Erwin, 1993; Alroy et al., 2008) and approximately 70% of species on land wiped out (Maxwell, 1992) within a short period of time, estimated at several hundred thousands of years or less (Mundil et al., 2004; Huang et al., 2011). Following the late Changhsingian mass extinction, there was a period of continued global climatic and environmental upheaval and stress termed the Early Triassic "cesspool" (e.g. Algeo 2011a) that lasted 5 million years and which was characterised by significant carbon isotope excursions, the global "coal gap", "reef gap", "radiolarian gap" and a range of unusual facies and biota including microbialites, and flat pebble conglomerates. This Early Triassic period of environmental upheaval was also characterised by significant size reduction of many organisms and is referred to in the literature as the period of "delayed recovery" following the mass extinction. The Early Triassic was also marked by significant variation in redox conditions both in time and space (Wignall and Twitchett, 2002; Kato et al., 2002; Kidder and Worsley 2004; Wignall et al., 2010) and by marked increase in chemical weathering intensity (Retallack and Krull, 1999; Michaelson, 2002; Sheldon, 2006; Algeo, 2011b; Algeo and Twitchett, 2010; Algeo et al., 2011). In shallow-marine environments there were frequent shifts between oxic and anoxic/dysoxic conditions, particularly in the Induan Stage (Bond and Wignall, 2010). These fluctuations of redox conditions have been interpreted to result from expansion of a shallow oxygen minimum zone into the ocean surface layer due to environmental perturbations (Algeo et al., 2011). The spatial and temporal mapping of these fluctuating redox conditions will greatly enhance our understanding of the causative environmental perturbations. We here review the

geographic and temporal variation of dysoxia and anoxia in both deep and shallow-marine environments globally, placing the recorded anoxia in the Perth Basin Hovea Member in wider context.

The latest Permian - Early Triassic in Western Australia includes economically important carbon-rich shallow-marine shales (Hovea Member, basal Kockatea Shale of the Perth Basin) that record dysoxic/anoxic conditions in the Early Triassic and which have acted as significant source rocks for hydrocarbons. The Late Changhsingian mass extinction and Permian-Triassic boundary levels also occur within the lower Hovea Mamber (Thomas and Barber, 2004; Thomas et al., 2004; Metcalfe et al., 2008; Gorter et al, 2009). The precise age of the Hovea Member has to date been poorly controlled and based mainly on endemic palynology and macro-fossils and limited conodont and ammonoid data. The specific placement of Permian -Triassic stage boundaries in Australia has until now been elusive or at best very poorly constrained. The Early Triassic Induan-Olenekian Stage boundary (Dienerian-Smithian sub-stage boundary) is yet to be formally ratified in a GSSP section by the Subcommission on Triassic Stratigraphy (STS). However, the STS has decided that the first appearance of the conodont *Neospathodus waageni* ex. gr. should be used for boundary definition and recognition in the GSSP (Tong et al., 2004; Krystyn et al., 2007; Tong and Zhao, 2011). The occurrence of Lower Triassic conodonts in Western Australia was first reported by McTavish (1973) in cores taken in petroleum exploration wells drilled in the Carnarvon and Perth basins. Smithian conodont faunas with *Neospathodus waageni* were recovered in the Carnarvon Basin and possible Dienerian strata in the Perth Basin based on a few *Neospathodus dieneri.* Additional limited conodont material from the Perth Basin (Metcalfe et al., 2008) failed to provide sufficient control to firmly place any stage boundary although the occurrence of *Clarkina jolfensis* Kozur in the basal Sapropelic Interval suggests that the biostratigraphic GSSP Permian-Triassic boundary level is within the lower part of the

Sapropelic Interval of the Hovea Member (Fig. 1). We here provide unequivocal placement of the proposed Induan-Olenekian boundary in the Perth Basin, Western Australia (Senecio-1 Core) based on relatively abundant conodont faunas. We also report $\delta^{13}C_{org}$ data from this boundary interval and correlate the studied sequence with proposed Induan-Olenekian GSSP sections in China and India and provide age constraints on post-mass extinction anoxia/dysoxia in Western Australia.

FIG 1 ABOUT HERE

2. Stratigraphy and geological setting of the studied sequence.

Permian-Triassic transitional sequences of Western Australia occur in the Perth, Carnarvon, Canning and Bonaparte continental margin basins. The Permian-Triassic transitional strata of these basins include thick marine shales that range from the latest Permian or earliest Triassic to as high as the early Anisian of the Middle Triassic (McTavish, 1973; McTavish and Dickins, 1974). In the Perth Basin the Kockatea Shale may be up to 1000 m thick, is usually black in color and becomes progressively less marine in its upper part (Mory & Iasky, 1996). The basal part of the Kockatea Shale in the Perth Basin has been named the Hovea Member (Thomas and Barber, 2004; Thomas et al., 2004) and consists of a basal Inertinitic Interval, a middle Sapropelic Interval and an upper Limestone Marker unit (Fig. 1). The Hovea Member is c.30-70 m thick and contains high total organic carbon (TOC) content up to 5% (Thomas and Barber, 2004; Thomas et al, 2004; Metcalfe et al., 2008). The bulk of the Kockatea Shale, above the Hovea Member, has a much lower average TOC of 0.8% (Mory & Iasky, 1996) perhaps reflecting high sedimentation rate.

The studied Induan-Olenekian boundary sequence is recorded in a core taken in

the onshore petroleum exploration well Senecio-1 drilled by Arc Energy Ltd in 2005 and located in the northern Perth Basin, east of Dongara at GPS coordinates Latitude 29 14 25.94 S, Longitude 115 05 29.28 E (see Fig. 1 for stratigraphic position and location). The Permian-Triassic transition in the Perth Basin (Fig. 1) occurs in the lower part of the Kockatea Shale (Hovea Member). The Hovea Member comprises a lower Inertinitic Interval (named for the high level of inert kerogen), a Sapropelic Interval (organic-rich mud with phytoplankton-derived kerogen) and an upper calcareous horizon termed the 'Limestone Marker' (Thomas et al. 2004). The Senecio-1 well penetrated the lower Hovea Member of the Kockatea Shale and bottomed in the Dongara Sandstone reservoir. The 21.6 m cored sequence (2708.00-2729.60 m depth) here studied straddles the upper Sapropelic Interval-lower 'Limestone Marker' section of the Hovea Member (Fig. 1). Carbon and sulfur isotopes and biomarker studies from the nearby Hovea-3 well (Thomas et al. 2004; Grice et al., 2005a; Grice et al., 2005b; Nabbefeld et al., 2010) indicate that the late Changhsingian mass extinction level corresponds to the Inertinitic Interval-Sapropelic Interval boundary and based on very limited conodont material and palynology, the biostratigraphic GSSP-defined Permian-Triassic boundary is placed in the lower part of the Sapropelic Interval (Metcalfe et al., 2008; Fig. 1). Isotope studies and biomarker data indicate periodic Photic Zone Euxinia (sulfidic conditions) at the time of deposition of the Sapropelic Interval in the Perth Basin and during the Late Permian-Early Triassic mass extinction and recovery interval globally (Grice et al., 2005a). Limited palynological studies (Purcell, 2006) indicate that the entire core falls within the Lower Triassic *Kraeuselisporites saeptatus* Zone. The Sapropelic Interval in the core (2721.70-2729.60 m) comprises organic C-rich (up to 2.5% TOC) finely laminated mudstones with rare thin generally sharp-based siltstones that represent an anoxic high-stand systems tract deposited on the distal shelf below storm wave base (Thomas et al., 2004). The mudstones and siltstones of the Sapropelic Interval show a high degree of pyritization and

contain pyrite nodules, pyrite spheres and framboids and pyritised microfossils (in particular common pyritised micro-bivalves and micro gastropods at some levels) are devoid of bioturbation (bioturbation index of 0) and contain no apparent infauna. Analysis of pyrite framboid size in the Hovea Member of the Kockatea Shale in Hovea-3 suggests anoxic conditions prevailed throughout the Late Permian and Early Triassic (Bond and Wignall, 2010). The smallest mean diameter pyrite framboids (4.5-5.1 µm) indicates that anoxia was most intense in the lower part of the Sapropelic Interval. This interval is interpreted to have been deposited under anoxic conditions. The upper part of the core (2708.00-2721.70 m) represents the upper Hovea Member "Limestone Marker" unit and comprises laminated mudstones with siltstones. Carbonate cemented intervals and concretions are common. The base of the unit is marked by a 40 cm thick sharp-based, fining-upwards, glauconitic siltstone that contains abundant largely broken and in some cases abraded *Clarkina* conodont Pa elements interpreted as transported. This and other siltstones in this unit are regarded as distal turbidites or tempestites (with mud rip-up clasts in places) deposited on the continental shelf below storm wave base but more shore proximal than the underlying Sapropelic Interval. Bioturbation is common, suddenly increasing to a Bioturbation Index (Bann and Fielding, 2004) of 4-5 (compared with 0 in underlying Sapropelic Interval) then gradually reducing with an upward deepening trend. Both horizontal and vertical burrows are present and the upper "Limestone marker" is considered to have been deposited in oxygenated conditions. The relatively rare and poorly preserved macro-fossils in the core are dominated by epifaunal pelagic thin-shelled bivalves and ammonites. Other epifauna commonly found in the cores include rare to abundant fish teeth and scales, small foraminifera, conodonts and ostracods.

3. Conodont faunas and the Induan-Olenekian boundary in Western Australia

3.1 Conodont samples and processing

Eighty seven samples, from top to bottom, C1 to C 87 (each 25 cm in length and c. 1 kg in weight) of a one-third slab of the Senecio-1 core were processed to extract conodonts. Samples were broken down by a variety of methods including treatment with hexane, dilute acetic/formic acid, sodium hypochlorite and sodium hydroxide. Residues were sieved and dried and then conodonts concentrated by heavy liquid (sodium polytungstate) and magnetic separation and picked under an optical binocular microscope. Imaging of conodonts was undertaken using a JEOL JSM- 6480 LA Scanning Electron Microscope at Macquarie University, Sydney.

3.2 Conodont fauna & maturity

The Senecio-1 conodont samples produced 1000+ conodont elements. Conodont yields varied from 0 to 200+ elements per sample. The conodont fauna is of relative low diversity with 10 species/subspecies of *Neospathodus* and two (possibly three) species of *Clarkina*. Taxonomic notes and comments on stratigraphically important conodonts are given below. The conodont Colour Alteration Indicex (CAI) of Senecio-1 elements is 2 to 2.5 and is consistent with spore color which gives a Staplin Thermal Alteration Index TAI averaging 3 but with a range 2+ to 4 (Purcell, 2006). This indicates that the Senecio-1 core sedimentary rocks are mature to over-mature but probably in the upper liquid window (Fig. 2).

FIG 2 ABOUT HERE

3.2.1 Taxonomic notes and comments

Only the Pa elements of selected taxa have been illustrated in this study. Material illustrated is currently reposited at the University of New England, Armidale, Australia.

FIG 3 ABOUT HERE

***Clarkina* spp.**

Fig. 3, 1-8.

We recognise several species of *Clarkina* in the Senecio-1 core material but have so far failed to classify these into known species. There may be up to three new species in our material and specific designation/description awaits further taxonomic work. We illustrate some typical Pa elements of this genus in Fig. 3.

FIG 4 ABOUT HERE

***Neospathodus dieneri* Sweet, 1970**

Fig. 4, 1-14.

Neospathodus dieneri is a well-known Early Triassic conodont species. Three morphotypes are recognised by some authors and used to designate sub-zones (e.g. Zhao et al., 2007). See Shigeta et al. (2009, p. 186) for recent synonomy. The species ranges from the early Dienerian to the middle Smithian but is most commonly found in the Dienerian where it

is used to designate a *Neospathodus dieneri* Zone (e.g. Tong et al., 2004, Orchard and Tozer, 1997).

FIG 5 ABOUT HERE

Neospathodus novaehollandiae McTavish, 1973

Fig. 5, 1-6.

This species was first described from the Carnarvon Basin of Western Australia by McTavish (1973). Some workers (e.g. Orchard, 2010) have placed this species in synonomy with *Neospathodus pakistanensis* but we here regard it as a separate species characterised by development of robust lateral flanges, developing into node like features in the posterior part of the element. None of the original McTavish material was illustrated by SEM. We here provide an SEM image of the Holotype Pa element (Fig. 5: 6) for comparison and it is identical to Pa elements recovered from the Senecio-1 Well. The species appears to be restricted to the Lower Olenekian (Smithian) and was used, together with *Neospathodus waageni* to define a basal Olenekian *Neospathodus* ex gr. *waageni* - *Neospathodus novaehollandiae* Zone in South Primorye, Russia (Shigeta et al., 2009).

Neospathodus pakistanensis Sweet, 1970

Fig. 6, 1-8.

Neospathodus pakistanensis is a long-established early Triassic conodont species first described from West Pakistan where it defines a *Neospathodus pakistanensis*

Zone that is succeeded by the *Neospathodus waageni* Zone. This species ranges from the late Dienerian (late Induan) to the middle Smithian (early Olenekian).

FIG 6 ABOUT HERE

Neospathodus ex gr. *waageni* Sweet 1970

Neospathodus waageni sensu lato is a long-established Smithian species, the first appearance of which has been chosen to define the base of the Olenekian Stage by the IUGS, ICS Subcommission on Triassic Stratigraphy. The species gives rise to several new *Neospathodus* species and species of *Novispathodus* in the early Spathian via the basal Spathian species *Neospathodus pingdingshanensis* (Orchard, 2007). Morphological variability in the species has led some authors to recognise up to six morphotypes (Orchard and Krystyn, 2007). Two subspecies, *Neospathodus waageni eowaageni* and *Neospathodus waageni waageni* were recognised by Zhao et al. (2008). We here recognise a third subspecies, *Neospathodus waageni* subsp. nov. A which is similar to, and possibly the ancestor of *Neospathodus pingdingshanensis.*

FIG 7 ABOUT HERE

Neospathodus waageni eowaageni Zhao et al., 2008

Fig. 7, 1-2.

Neospathodus waageni eowaageni is the oldest subspecies and is characterised by a shorter element and upright denticles. The subspecies is rare compared to *Neospathodus*

waageni waageni and has its first occurrence before *Neospathodus waageni waageni* in all proposed Induan-Olenekian GSSP sections studied in China, India and Russia and in the Senecio-1 Well, Australia. The sub-species has a very short range at the base of the Olenekian and defines a short-duration *Neospathodus waageni eowaageni* Zone which is succeeded upwards by the first appearance of *Neospathodus waageni waageni* defining the base of the *Neospathodus waageni waageni* Zone.

***Neospathodus waageni waageni* Sweet 1970**

Fig. 8, 1-9.

This is the commonest subspecies, characterised by its typical reclined denticles. We do not here recognise any morphotypes. The subspecies ranges from just above the base of the Olenekian to the top of the Smithian sub-stage.

FIG 8 ABOUT HERE

***Neospathodus waageni* subsp. nov. A**

Fig. 9, 1-9.

This proposed subspecies appears some distance above the base of the *Neospathodus waageni waageni* Zone and is relatively common. It is characterised by denticles that are curved towards the posterior similar to those in *Neospathodus pingdingshanensis*. The sub-species also exhibits wider and broader striations on the denticles compared to other sub-species. We here utilise this subspecies to define a *Neospathodus waageni* subsp. nov. A Sub-Zone in the Senecio-1 succession.

FIG 9 ABOUT HERE

3.3. Conodont zonation and the Induan-Olenekian boundary

The critical age- and zonal-indicative species and sub-species discussed above allow the unequivocal placement of the proposed Induan-Olenekian boundary at 2719.25 m depth in the core (in the lower part of the "Limestone marker" unit). The ranges and relative abundance of important conodont taxa and conodont zonation are given in Fig. 10. Three Zones and one Sub-Zone are recognised in the core in ascending order:

***Neospathodus dieneri* Zone (2719.25-2729.60 m)**:

Characterised by the co-ocurrence of *Neospathodus pakistanensis* and *Clarkina* spp..

***Neospathodus waageni eowaageni* Zone (2717.25-2719.25 m)**:

Characterised by the co-occurrence of *Neospathodus waageni eowaageni* and *Clarkina* spp. and the base defined by the first occurrence of *Neospathodus waageni eowaageni.*

FIG 10 ABOUT HERE

***Neospathodus waageni waageni* Zone (2708.00-2717.25 m)**:

Characterised by the zonal name species together with *Neospathodus dieneri*, *Neospathodus novaehollandiae*, and *Neospathodus pakistanensis*. Base defined by first appearance of *Neospathodus waageni waageni.*

***Neospathodus waageni* subsp. nov. A Sub-Zone (2708.00-2715.00 m)**:

Corresponds to the upper part of the *Neospathodus waageni waageni* Zone and characterised by the occurrence of *Neospathodus waageni* subsp. nov. A.

The first appearance of *Neospathodus waageni* ex. gr. (sensu lato) is used to define the base of the proposed Olenekian Stage of the Lower Triassic (Tong et al., 2004; Krystyn et al., 2007; Tong and Zhao, 2011). This corresponds to the first appearance of *Neospathodus waageni eowaageni* in proposed GSSP sections at Chaohu, China (Zhao et al., 2007; Zhao et al., 2008; Tong and Zhao, 2011) and Mud, Spiti, India (Krystyn et al., 2007; Orchard and Krystyn, 2007; Tong et al., 2011) and to the first appearance of *Neospathodus waageni* ex. gr. (sensu lato) in other Induan-Olenekian boundary sections globally, e.g. Abrek Bay, South Primorye (Shigeta et al., 2009), The first appearance of *Neospathodus waageni eowaageni* occurs slightly before the appearance of *Neospathodus waageni waageni* in the proposed GSSP sections and this is also the case in the Senecio-1 core in the Perth Basin. We here place the Induan-Olenekian Stage (Dienerian-Smithian Sub-Stage) boundary at this first appearance in the core at a depth of 2719.25 m. This is the first unequivocally established international stage boundary in the Permian and Triassic of Australia.

4. Carbon Isotopes

TABLE 1 ABOUT HERE

4.1. Analytical methodology

4.1.1. Sample preparation

The samples were surface washed with a mixture of dichloromethane (DCM) and methanol (CH_3OH) [9:1, vol%: vol%] in an ultrasonic bath (20 min) to remove surface contamination. The air-dried samples were then ground to a particle size of approximately 150 µm using a ring mill.

4.1.2 Elemental analysis-isotope ratio mass spectrometry (EA-irm-MS)

To remove inorganic carbon from the ground samples for $\delta^{13}C$ of bulk organic matter (OM) analysis, the ground samples were acidified with Hydrochloric acid (HCl,1Molar) and then oven-dried at approximately 40^{o}C [48h] in an oven. Then the samples were washed at least three times with double-distilled water to remove any remaining HCl. These decarbonised samples were measured for $\delta^{13}C$ of bulk OM analysis using a Micromass IsoPrime isotope ratio mass spectrometer interfaced to a EuroVector EuroEA3000 elemental analyser.

The samples were combusted (1025 ^{o}C) under an oxygen-enriched atmosphere. Subsequently, the composition products were transported *via* a constant helium flow through an oxidation catalyst (chromium oxide) into a reduction reactor (650 ^{o}C) containing copper granules to reduce nitrogen oxides (NO, N_2O and N_2O_2) to N_2. Excess oxygen and water were removed. Remaining CO_2 and N_2 were separated on a 3m chromatographic column (Poropak Q) before the gas was transported through a thermal conductivity detector (TCD) and into the isotope ratio mass spectrometer (ir-MS). For more detail of the procedure see Grice et al. (2007). Isotopic compositions are given in the δ-notation relative to the Vienne Pee Dee Belemnite (VDPB) standard.

TABLE 1 ABOUT HERE

4.1.3. Isotope values and interpretation

$\delta^{13}C_{org}$ values vary from -27.52 to -32.91 ‰ VPDB (Table 1) and define a broad positive excursion of approximately 4 per mille (Fig. 11). The peak of this excursion essentially coincides with the base of the *Neospathodus waageni eowaageni* Zone and hence the biostratigraphically defined Induan-Olenekian boundary in the core. Similar positive $\delta^{13}C_{carb}$ excursions have been reported globally (Corsetti et al., 2005) and from proposed marine GSSP sections at West and North Pingdingshan, Chaohu, China, and at Mud, Spiti, India (Tong et al., 2002; Horacek et al., 2007; see Fig. 4). In addition, positive excursions are also known at other Induan-Olenekian boundary sections including Jinya/Waili, northwestern Guangxi, South China (Galfetti et al., 2007a), Daxiakou Section, Hubei, China (Tong et al., 2002), Guandao section, Guizhou, China (Tong et al., 2002), Zuodeng Section, Tiandong, Guangxi Province, China (Tong et al., 2002), Bulla section, Southern Alps, Italy (Posenato, 2008), L´Om Picol/Uomo section, northern Italy (Horacek et al., 2007), Losar, North India (Galfetti et al., 2007b) and Kamura, Japan (Horacek et al., 2009).

FIG 11 ABOUT HERE

5. Global anoxia/dysoxia in the Late Permian-Early Triassic

FIG 12 ABOUT HERE

The Late Permian-Early Triassic is characterised by significant global development of marine dysoxia (low oxygen concentration), anoxia (water and sediments

lacking oxygen) and euxinia (sulfidic anaerobic conditions with sulphate-reducing bacteria leading to accumulation of organic-rich black shales).

Evidence that indicates dysoxia/anoxia in the Permian-Triassic transitional interval includes lithostratigraphy (Wignall and Twitchett, 1996, 2002; Isozaki, 1997), sulfur isotopes (Newton et al, 2004; Nielsen and Shen, 2004), occurrence and size distribution of framboidal pyrite (Nielsen and Shen, 2004; Wignall et al., 2005; Gorjan et al., 2007; Bond and Wignall, 2010), trace metal distributions (Kakuwa, and Matsumoto, 2006; Kakuwa, 2008), type or total lack of biotubation (Twitchett and Wignall, 1996; Kakuwa, 2008), low-diversity, thin-shelled benthic faunas (Wignall and Twitchett, 2002), S/C ratio distributions (Gorjan et al., 2007), high levels of Total Organic Carbon (Takahashi et al., 2009).

5.1. Western Tethys

Wignall and Twitchett (2002) indicate anoxic conditions for the Griesbachian in deep-water, deep basin sequences of Sicily, Italy. In shallow marine environments, Newton et al. (2004) based on $\delta^{34}S$ and $\delta^{18}O$ studies of sediments in the Permian-Triassic of Siusi, in the dolomites of northern Italy indicate anoxia in the latest Permian and Griesbachian. Dysoxic conditions in the post extinction latest Permian and Griesbachian are indicated by trace fossil, geochemical and sedimentological data (Wignall and Hallam,1992; Twitchett and Wignall, 1996; Twitchett, 1999). Dolenec et al. (2001) using redox sensitive elements, S, C, REE distributions and Ce anomaly data in Permian-Triassic shallow-marine sediments in western Slovenia interpret anoxic conditions in the latest Permian and oxic/dysoxic conditions in the Griesbachian. Gorjan et al (2007) discuss palaeoredox conditions in the Bulla section, northern Italy and again interpret anoxia in the latest Permian and Griesbachian.

5.2. Eastern Tethys

Deep-marine basin sequences in N. Sichuan, China record anoxia from the latest Changhsingian (extinction level) to the early Dienerian (Wignall and Twitchett, 2002). In the shallow-marine low-latitude environment in South China (Meishan) anoxia commenced at the extinction horizon (top of Bed 24) but then fluctuated between oxic, dysoxic and anoxic in the basal Induan (Bond and Wignall, 2010). Biomarker studies indicate periodic photic zone euxinia in the latest Permian and Griesbachian at Meishan (Grice et al., 2005a). Kershaw et al (1999) indicate probable onset of anoxic/dysoxic conditions at the extinction level based on a sudden increase in pyrite, appearance of pyrite framboids, micro-gastropods and microsperes in the Baizhuyuan section, Sichuan Province, South China. Galfetti et al. (2007b) interpret two periods of dysoxia-anoxia in the Jinya/Waili sections of SW South China, one in the Griesbachian-Dienerian and one in the Smithian.

5.3. Panthalassa

Data from deep ocean floor sediments of Panthalassa now incorporated into accretionary complexes in Japan led Kajiwara et al. (1993a, 1993b, 1994) based on δ^{34} S data and Kato et al. (2002) using lithostratigraphic and geochemical data (major, trace and rare earth elements, including Ce anomaly) to interpret the onset of dysoxic conditions in the Wuchiapingian and anoxic conditions from the late Changhsingian (mass extinction level) into the lower Induan (Griesbachian). Wignall et al. (2010) also proposed dysoxic conditions in late Permian deep-marine Panthalassic sediments of accreted terranes in Japan and appearance of distinct anoxia at the late Changhsingian extinction horizon that extends through the Griesbachian. A further pulse of anoxia is recorded in the late Spathian.

In the shallow-water central Panthalassa (sea mounts incorporated into accretionary complexes in Japan), geochemical signatures in dark-grey to black Griesbachian micritic limestones indicate dysoxic conditions at this time on shallow-marine intra-Panthalassic sea mounts (Musashi et al, 2001). Shallow marine higher-latitude eastern Panthalassa continental margin sequences in Idaho, W. North America record anoxia from the extinction level up into the Griesbachian (Wignall and Hallam,1992; Bond and Wignall, 2010). Dysoxia in the Griesbachian of Utah and Idaho is indicated by abundant *Lingula* and *Claraia* (Schubert and Bottjer (1995). Photic zone euxinia is documented in the latest Permian, Griesbachian and Smithian in the Peace River Basin, Western Canada (Hays et al 2007).

5.4. Peri-Gondwana

Brookfield et al. (2003) suggest there is little evidence for dysaerobic conditions in the deep-water P-T transition in the Guryul Ravine and Pahlgam sections in Indian Kashmir. However, the lower Khunamuh Formation (upper Permian-basal Triassic) lacks bioturbation and Wignall et al (2005), based on pyrite framboid evidence, have interpreted this to have been deposited under oxygen poor conditions.

In shallow-marine Peri-Gondwana P-T sequences at Julfa, Iran, dysoxic conditions in the Griesbachian are indicated by Ce anomaly studies (Kakuwa and Matsumoto, 2006). In the Salt Range, Pakistan, Wignall and Hallam (1993) indicate early Griesbachian normal marine conditions but dysoxic conditions in the late Griesbachian. Hermann et al. (2011) assessed the palaeoredox data for the Salt Range and Surghar Range sections in Pakistan and interpret, based on composition of organic particulate matter, that oxygenated conditions existed in the Early Triassic except in the Dienerian-earliest Smithian and

challenge the interpretation of an anoxic event in the late Griesbachian. They indicate dysoxic conditions throughout the Dienerian and in the late Smithian (Hermann et al. 2011, Fig 9). The Triassic sequence at Losar, India records two episodes of anoxia, one in the late Dienerian and one in the late Smithian separated by dysoxic conditions (Galfetti et al., 2007a).

At Selong, Southern Tibet, Wignall and Newton (2003) demonstrate that the basal Triassic is oxygenated and dysoxic conditions only appear in the late Griesbachian and anoxic conditions in the Dienerian.

Peri-Gondwanan shallow-marine P-T sequences are present in the Perth, Carnarvon and Bonaparte basins of Western Australia. Biostratigraphic control is mainly based on endemic palynomorphs, brachiopods and bivalves and on limited more globally relevant conodonts and ammonoids. Metcalfe et al. (2008) and Gorter et al. (2009) discussed the placement of the P-T boundary in the Perth and Bonaparte basins. The Griesbachian is yet to be unequivocally proved present in any of these sequences based on international robust biostratigraphy but is generally regarded as probably present in the Perth Basin (Thomas et al 2004, Metcalfe et al, 2008) but with the possibility of a stratigraphic break at the extinction level (Inertinitic Interval-Sapropelic Interval boundary). The presence of the Griesbachian in the Carnarvon and Bonaparte basins is also equivocal and as yet unproven. The latest Permian and basal Triassic appear missing in the Carnarvon Basin where there is an unconformity (Felton et al., 1993). The Lower Triassic in the Carnarvon Basin is represented by the Locker Shale but there is no indication of oxygen deficient conditions at that time or in the underlying Permian Kennedy Group. There is also an unconformity present in the latest Permian in the Bonaparte Basin (Gorter et al., 2009) but this occurs below the *Protohaploxypinus microcorpus* palynofloral Zone interpreted as of late but not latest Changhsingian age (Metcalfe et al, 2008). The Griesbachian may be represented within the

Mairmull Formation in the Bonaparte Basin. There is no indication of dysoxia or anoxia in the Permian-Triassic transitional interval in the Bonaparte Basin and the organic-rich source rocks of the lower Triassic seen in the Perth Basin are not present there.

Anoxic conditions are interpreted for the Sapropelic Interval of the Hovea Member of the Kockatea Shale in the Perth Basin (Thomas et al 2004, Metcalfe et al., 2008, and discussions in this paper) commencing at the late Changhsingian extinction level and terminating in the late Dienerian. In addition, biomarker studies indicate photic zone euxinia during deposition of the Sapropelic Interval of the Kockatea Shale (Grice et al., 2005a).

6. Discussion

The development of global anoxia has been suggested to be a primary cause of the late Changhsingian marine mass extinction (Wignall and Hallam, 1992; Isozaki, 1997; Wignall & Twitchett 2002). The development of dysoxia and anoxia in the Permian-Triassic transition exhibits both depth-related and geographic variations (Fig. 12). It has previously been suggested that dysoxia and anoxia in the deep-marine environment commences in the late Middle Permian (late Capitanian) and extends to the early Middle Triassic (early Anisian) and has been referred to as a long-lasting "superanoxic event" (Kajiwara et al., 1994; Isozaki, 1997; Kato et al., 2002; Isozaki, 2009). Oceanic stagnation during this "superanoxic event" has been shown, based on modeling, to be unlikely (Hotinski et al., 2001; Winguth and Maier-Reimer, 2005). Biomarker and C and S isotope studies in China, Australia, Greenland and Western Canada (Grice et al., 2005a; Hays et al., 2006; Hays et al., 2007) have indicated that widespread periodic photic-zone sulfidic conditions (photic zone euxinia) existed during this "superanoxic event" and that sulfide toxicity was a contributory factor to the extinction and a factor in delayed recovery in the early Triassic. Earth system modeling (Meyer et al,

2008) suggests that H_2S toxicity and hypercapnia may have provided the kill mechanism for the P-T extinction. Photic-zone sulfidic conditions as a principal cause for the late Changhsingian ecosystem collapse and mass extinction is more problematic and has been recently challenged by Nielsen et al. (2010). Anoxia in the pre-extinction Late Permian has been interpreted, based on modeling, to not have been globally widespread but confined to an oxygen minimum zone and the deep eastern Panthalassa (Winguth and Winguth, 2011). Anoxia in the shallow-marine environment appeared in the latest Permian at the extinction level (Fig. 12), later than in the deep-marine environment, and appears to be largely restricted to the Induan (Griesbachian and Dienerian) and early Olenekian (Smithian). Extreme global warming ocurred in the latest Permian-early Triassic, immediately post-mass extinction (Joachimski et al., 2012), with major changes in the Earth's ocean and atmosphere heat transfer systems (Kidder and Worsley, 2004). Pulses of shallow-marine anoxia during the Induan-Early Olenekian correspond to major global positive $\delta^{13}C$ isotopic excursions (Fig. 12) and are suggested to be caused by repeated expansion of the oxygen minimum zone into the ocean surface layer due to environmental perturbations (Algeo 2011a, 2011b) including extreme global warming, increased chemical weathering intensity and continental erosion, sea level rise, and changes in marine nutrient inventories and productivity rates (Algeo et al., 2011).

Wignall & Twitchett (2002) discussed the temporal and spatial distribution of both deep- and shallow-marine anoxia globally and indicated that oxygen-poor shallow-marine conditions widely developed in the latest Changhsingian and was at its maximum in the mid-Griesbachian and had waned by the mid-Dienerian to low-latitude areas of Panthalassa and a region of peri-Gondwana in a shallow-marine embayment in the India-Madagascar region. Better constraints on the spatial distribution and upper limit of shallow-marine anoxia in the Early Triassic are now available and our new data from the Perth Basin

in Western Australia expands the known region of Induan shallow-marine anoxia in the peri-Gondwanan Meso-Tethys and dates its termination as late Dienerian. A compilation of currently available data on shallow-marine anoxia/dysoxia (Fig. 12) demonstrates synchronous establishment of dysoxia/anoxia at the Late Changhsingian mass extinction level but different timings of the cessation of anoxia in different palaeogeographical regions and settings. It is not yet clear if different temporal pulses of anoxia in the shallow-marine environment are global or regional in nature. Thomas et al. (2004) suggested that upwelling on the west Australian Gondwana margin resulted in abnormally high productivity that produced the unique Lower Triassic organic-rich source rocks of the Sapropelic Interval of the Hovea Member of the Kockatea Shale. This upwelling may also explain the relatively late cessation (late Dienerian) of anoxia along this part of the peri-Gondwana margin. Another possible explanation for the anoxia and organic-rich source rocks of the Sapropelic Interval of the Hovea Member is increased surface ocean productivity due to restricted water circulation and photic zone euxinia (Grice et al., 2005b). Further detailed temporal and spatial mapping of anoxia in the Late Permian-Early Triassic will lead to further understanding of the driving forces for anoxia and how environmental perturbations both on-land and in the seas underpinned these forces.

7. Conclusions

Conodont biostratigraphy has unequivocally established the Induan-Olenekian Stage (Dienerian-Smithian Sub-stage) boundary in the Permo-Triassic succession of the onshore northern Perth Basin, Australia, specifically in the lower part of the "Limestone Marker" of the Hovea Member of the Kockatea Shale cored in the petroleum exploration well

Senecio 1. This is the first unequivocally established Stage boundary for either the Permian or Triassic of Australia utilising internationally robust biostratigraphy.

$\delta^{13}C_{org}$ values from the Induan-Olenekian transition in the Perth Basin vary from -27.52 to -32.91 ‰ VPDB and define a broad positive excursion of approximately 4 per mille. This correlates with a globally recognised positive excursion at this level and enhances correlation of the Senecio-1 section conodont zonation with proposed Induan-Olenekian GSSP sections in China and India and demostrates the utility of this conodont defined level for stage boundary definition and global correlation.

The upper limit of anoxic conditions recognised in the Sapropelic Interval of the Hovea Member of the Kockatea Shale, Perth Basin is dated as late Induan (late Dienerian). Temporal and spatial mapping of marine anoxia and dysoxia globally demonstrates that pulses of anoxia affected shallow-marine zones at different times in different locations. This was probably caused by repeated expansion and/or geographically restricted upwelling of an oxygen minimum zone into the ocean surface layer due to environmental perturbations including extreme global warming, increased terrestrial chemical weathering intensity and continental erosion, sea level rise, and changes in marine nutrient inventories and productivity rates.

Acknowledgments

IM and RSN were supported by Australian Research Council Discovery Grant DP109288. KG and ML were supported by ARC QEII Discovery grant to KG. ML was supported by Geoscience Australia, GFZ Potsdam and Curtin University for a Curtin International Tuition Scholarship. The Institute for Geoscience Australia and John de Le State Centre provided support. The authors wish to extend their thanks to Arc Energy Ltd, now AWE Ltd, and its joint venture partner Origin Energy Ltd for permission to access its Senecio

1 core for research. Paul Wignall and Charles Henderson are thanked for their helpful reviews of the paper.

References

Algeo, T.J. 2011a. The Early Triassic cesspool: Marine conditions following the end-Permian mass extinction. In: Håkansson, E., Trotter, J. (Eds), Programme & Abstracts, The XVII International Congress on the Carboniferous and Permian, Perth 3–8 July 2011: Geological Survey of Western Australia, Record 2011/20, 38.

Algeo, T.J. 2011b. Enhanced continental weathering in the latest Permian to Early Triassic: Effects on shallow marine biotas. In: Håkansson, E., Trotter, J. (Eds), Programme & Abstracts, The XVII International Congress on the Carboniferous and Permian, Perth 3–8 July 2011: Geological Survey of Western Australia, Record 2011/20, 38.

Algeo, T.J., Twitchett, R.J., 2010. Anomalous Early Triassic sediment fluxes due to elevated weathering rates and their biological consequences. Geology 38, 1023-1026.

Algeo, T., Chen, Z.Q., Fraiser, M.L., Twitchett, R.J., 2011. Terrestrial–marine teleconnections in the collapse and rebuilding of Early Triassic marine ecosystems. Palaeogeography, Palaeoclimatology, Palaeoecology 308, 1-11.

Alroy, J., Aberhan, M., Bottjer, D.J., Foote, M., Fürsich, F.T., Harries, P.J., Hendy, A.J.W., Holland, S.M., Ivany, L.C., Kiessling, W., Kosnik, M.A., Marshall, C.R., McGowan, A.J., Miller, A.I., Olszewski, T.D., Patzkowsky, M.E., Peters, S.E., Villier, L., Wagner, P.J., Bonuso, N., Borkow, P.S., Brenneis, B., Clapham, M.E., Fall, L.M., Ferguson, C.A., Hanson, V.L., Krug, A.Z., Layou, K.M., Leckey, E.H., Nürnberg, S., Powers, C.M., Sessa, J.A., Simpson, C., Tomašových, A., Visaggi, C.C., 2008. Phanerozoic trends in the global diversity of marine invertebrates. Science 321, 97–100.

Bann, K.L., Fielding, C.R., 2004 . An integrated ichnological and sedimentological comparison of non deltaic shoreface and subaqueous delta deposits in Permian reservoir units of Australia. In McIlroy, D. (Ed), The Application of Ichnology to Palaeoenvironmental and Stratigraphic Analyis. Geological Society of London, Special Publication 228, 273-310.

Bond, D.P.G., Wignall, P.B., 2010. Pyrite framboid study of marine Permian–Triassic boundary sections: A complex anoxic event and its relationship to contemporaneous mass extinction. Geological Society of America Bulletin 122, 1265–1279.

Brayard, A., Vennin, E., Olivier, N., Bylund, K.G., Jenks, J., Stephen, D.A., Bucher, H., Hofmann, R., Goudemand, N., Escarguel, G., 2011. Transient metazoan reefs in the aftermath of the end-Permian mass extinction. Nature Geoscience 4, 693-697.

Brookfield, M.E., Twitchett, R.J., Goodings, C., 2003. Palaeoenvironments of the Permian-Triassic transition sections in Kashmir, India. Palaeogeography, Palaeoclimatology, Palaeoecology 198, 353-371.

Corsetti, F.A., Baud, A., Marenco, P.J., Richoz, S., 2005. Summary of Early Triassic carbon isotope records. Comptes Rendus Palevol 4, 473-486.

Dolenec, T., Lojen, S., Ramovs, A., 2001. The Permian–Triassic boundary in Western Slovenia (Idrijca Valley section): magnetostratigraphy, stable isotopes, and elemental variations. Chemical Geology 175, 175–190.

Epstein, A.G., Epstein, J.B., Harris, L.D., 1977. Conodont color alteration; an index to organic metamorphism. U.S. Geological Survey Professional Paper 0995, 27 pp.

Erwin, D.H. 1993. *The Great Paleozoic Crisis.* Columbia Univ. Press, New York.

Felton, E.A., Miyazaki, S., Dowling, L. Pain, L., Vuckovic V., le Poidevin, S.R., 1993. *Carnarvon Basin, W.A.*, Bureau of Resource Sciences, Australian Petroleum Accumulations Report 8.

Galfetti, T., Bucher, H., Brayard, A., Hochuli, P.A., Weissert, H., Guodun, K., Atudorei, V., Guex, J., 2007a. Late Early Triassic climate change: insights from carbonate carbon isotopes, sedimentary evolution and ammonoid paleobiogeography. Palaeogeography, Palaeoclimatology, Palaeoecology 243, 394–411.

Galfetti, T., Bucher, H., Ovtcharova, M., Schaltegger, U., Brayard, A., Bruhwiler, T., Goudemand, N., Weissert, H., Hochuli, P.A., Cordey, F., Guodun, K., 2007b. Timing of the Early Triassic carbon cycle perturbations inferred from new U–Pb ages and ammonoid biochronozones. Earth and Planetary Science Letters 258, 593–604.

Gorjan, P., Kaiho, K., Kakegawa, T., Niitsuma, S., Chen, Z.Q., Kajiwara., Nicora, A., 2007. Paleoredox, biotic and sulfur-isotopic changes associated with the end-Permian mass extinction in the western Tethys. Chemical Geology 244, 483–492.

Gorter, J.D., Nicoll, R.S., Metcalfe, I., Willink, R.J. and Ferdinando, D. 2009. The Permian-Triassic boundary in western Australia: evidence from the Bonaparte and Northern Perth basins: exploration implications. Australian Petroleum Production & Exploration Association Journal 2009, 311-336.

Grice K., Cao C., Love G. D., Bottcher M. E., Twitchett R. J., Grosjean E., Summons R. E., Turgeon S. C., Dunning W., Jin Y., 2005a. Photic zone euxinia during the Permian – Triassic Superanoxic Event. Science 307, 706 – 709.

Grice K., Summons R. E., Grosjean E., Twitchett R. J., Dunning W., Wang, S.X., Bottcher, M.E., 2005b. Depositional conditions of the northern onshore Perth Basin (basal Triassic). Australian Petroleum Production and Exploration Association Journal 45, 263-273.

Grice, K., Nabbefeld, B., Maslen, E., 2007. Source and significance of selected polycyclic aromatic hydrocarbons in sediments (Hovea-3 well, Perth Basin, Western Australia) spanning the Permian-Triassic boundary. Organic Geochemistry 38, 1795-1803.

Hays, L., Love, G.D., Foster, C.B., Grice, K., Summons, R.E., 2006. Lipid biomarker records across the Permian-Triassic boundary from Kap Stosch, Greenland: Eos (Transactions, American Geophysical Union) 87, no. 52, PP41B–1203.

Hays, L.E., Beatty, T., Henderson, C.M., Love, G.D., Summons, R.E., 2007. Evidence for photic zone euxinia through the end-Permian mass extinction in the Panthalassic Ocean (Peace River Basin, Western Canada): Paleoworld 16, 39–50.

hwiler, T., Ware, D., Hautmann, M., Roohi, G., ur-Rehman, K., Yaseen, A., 2011. Organic matter and palaeoenvironmental signals during the Early Triassic biotic recovery: The Salt Range and Surghar Range records. Sedimentary Geology 234, 19–41.

Horacek, M., Brandner, R., Abart, R., 2007. Carbon isotope record of the P/T boundary and the Lower Triassic in the Southern Alps: evidence for rapid changes in storage of organic carbon. Paleogeography, Paleoclimatology, Paleoecology 252, 347–354.

Horacek, M., Koike, T., Richoz, S., 2009. Lower Triassic $\delta^{13}C$ isotope curve from shallow-marine carbonates in Japan, Panthalassa realm: Confirmation of the Tethys $\delta^{13}C$ curve. Journal of Asian Earth Sciences 36, 481–490.

Hotinski, R.M., Bice, K.L., Kump, L.R., Najjar, R.G., Arthur, M.A., 2001, Ocean stagnation and end-Permian anoxia. Geology 29, 7–10.

Huang, C., Tong, J., Hinnov, L., Chen, Z.Q., 2011. Did the great dying of life take 700 k.y.? Evidence from global astronomical correlation of the Permian-Triassic boundary interval. Geology 39, 779-782.

Isozaki, Y., 1997. Permo-Triassic boundary superanoxia and stratified superocean: Records from lost deep sea. Science 276, 235-238.

Isozaki, Y. 2009. Integrated ‘‘plume winter” scenario for the double-phased extinction during the Paleozoic–Mesozoic transition: The G-LB and P-TB events from a Panthalassan

perspective. Journal of Asian Earth Sciences 36, 459–480.

Joachimski, M.M., Lai, X., Shen, S., Jiang, H., Luo, G., Chen, J., Sun, Y., 2012. Climate warming in the latest Permian and the Permian–Triassic mass extinction. Geology 40, 195–198.

Kajiwara, Y., Ishida, K., Tanikura, Y., Ishiga, H., 1993a. Sulfur isotope data from the Permian-Triassic boundary at Sasayama in the Tanba Terrane in southwestern Honshu, Japan. Annu. Rep. Inst. Geosci., Univ. Tsukuba 19, 67–72.

Kajiwara, Y., Yamakita, S., Kobayashi, D., Imai, A., 1993b. Sulfur isotope data from the Permian-Triassic boundary at Tenjinmaru in the Chichibu Terrane in eastern Shikoku, Japan. Annu. Rep. Inst. Geosci., Univ. Tsukuba 19, 59–66.

Kajiwara, Y., Yamakita, S., Ishida, K., Ishida, H., Imai, A., 1994. Development of a largely anoxic stratified ocean and its temporary massive mixing at the Permian/Triassic boundary supported by the sulfur isotopic record. Palaeogeography, Palaeoclimatology, Palaeoecology 111, 367-379.

Kakuwa, Y., 2008. Evaluation of palaeo-oxygenation of the ocean bottom across the Permian–Triassic boundary. Global and Planetary Change 63, 40–56.

Kakuwa, Y., Matsumoto, R., 2006. Cerium negative anomaly just before the Permian and Triassic boundary event — The upward expansion of anoxia in the water column. Palaeogeography, Palaeoclimatology, Palaeoecology 229, 335– 344.

Kato, Y., Nakao, K., Isozaki, Y., 2002. Geochemistry of Late Permian to Early Triassic pelagic cherts from southwest Japan: implications for an oceanic redox change. Chemical Geology 182, 15–34.

Kershaw, S., Zhang, T., Lan, G., 1999. A ?microbialite carbonate crust at the Permian–Triassic boundary in South China, and its palaeoenvironmental significance. Palaeogeography, Palaeoclimatology, Palaeoecology 146, 1–18.

Kidder, D.L., Worsley, T.R., 2004. Causes and consequences of extreme Permo-Triassic warming to globally equable climate and relation to the Permo-Triassic extinction and recovery. Palaeogeography, Palaeoclimatology, Palaeoecology 203, 207-237.

Knoll, A.H., Bambach, R.K., Payne, J.L., Pruss, S., Fischer, W.W., 2007. Paleophysiology and end-Permian mass extinction: Earth and Planetary Science Letters 256, 295–313.

Kozur, H., 1990. The taxonomy of the gondolellid conodonts in the Permian and Triassic. Cour. Forsch. Inst. Senckenberg 117, 409–469.

Krystyn, L., Bhargava, O. N., Richoz, S., 2007. A candidate GSSP for the base of the Olenekian Stage: Mud at Pin Valley; district Lahul & Spiti, Himachal Pradesh (Western Himalaya), India. Albertiana, 35, 5-29.

Lehrmann, D.J., Ramezani, J., Bowring, S.A., Martin, M.W., Montgomery, P., Enos, P., Payne, J.L., Orchard, M.J., Wang, H., Wei, J.Y., 2006. Timing of recovery from the end-Permian extinction: geochronologic and biostratigraphic constraints from South China. Geology 34, 1053–1056.

Maxwell, W.D. 1992. Permian and Early Triassic extinction of non-marine tetrapods. Palaeontology 35, 571-583.

McTavish, R. A., 1973. Triassic conodont faunas from Western Australia. Neues Jahrbuch fur Geologie und Palaontologie Abhandlungen 143, 275 – 303.

McTavish, R. A., Dickins, J.M., 1974. The age of the Kockatea Shale (Lower Triassic), Perth Basin—a reassessment. Journal of the Geological Society of Australia, 21, 195-201.

Metcalfe, I., Nicoll, R.S., Willink, R.J., 2008. Conodonts from the Permian Triassic transition in Australia and position of the Permian-Triassic boundary. Australian Journal of Earth Sciences 55, 349 – 361.

Metcalfe, I., Riley, N.J., 2010. Conodont Colour Alteration pattern in the Carboniferous of the Craven Basin and adjacent areas, northern England. Proceedings of the Yorkshire

Geological Society 58, 1-9.

Meyer, K.M., Kump, L.R., Ridgwell, A., 2008. Biogeochemical controls on photic-zone euxinia during the end-Permian mass extinction. Geology 36, 747–750.

Michaelson, P., 2002. Mass-extinction of peat-forming plants and the effect on fluvial styles across the Permian–Triassic boundary, northern Bowen Basin, Australia. Palaeogeography, Palaeoclimatology, Palaeoecology 179, 173–188.

Mory, A.J., Haig, D.W., McLoughlin, S., Hocking, R., 2005. Geology of the northern Perth Basin, Western Australia — a field guide: Western Australia Geological Survey, Record 2005/9, 71p.

Mory, A. J., Iasky, R. P., 1996. Stratigraphy and structure of the onshore northern Perth Basin, Western Australia. Western Australia Geological Survey, Report 46, 101p.

Mundil, R., Ludwig, K.R., Metcalfe, I., Renne, P.R., 2004. Age and Timing of the Permian Mass Extinctions: U/Pb Geochronology on Closed-System Zircons. Science 305, 1760-1763.

Mundil, R., Palfy, J., Renne, P.R., Brack, P., 2010. The Triassic time scale: new constraints and a review of geochronological data. In: Lucas, S.G. (Ed.), The Triassic Timescale. Geological Society of London Special Publication 334, 41–60.

Musashi, M., Isozaki, Y., Koike, T., Kreulen, R., 2001. Stable carbon isotope signature in mid-Panthalassa shallow-water carbonates across the Permo-Triassic boundary: evidence for ^{13}C-depleted superocean. Earth and Planetary Science Letters 191, 9-20.

Nabbefeld, B., Grice, K., Schimmelmann, A., Sauer, P.E., Böttcher, M.E., Twitchett, R., 2010. Significance of $\delta D_{kerogen}$, $\delta^{13}C_{kerogen}$ and $\delta^{34}S_{pyrite}$ from several Permian/Triassic (P/Tr) sections. Earth and Planetary Science Letters 295, 21–29.

Newton, R., Pevitt, E.L., Wignall, P.B., Bottrell, S.H., 2004. Large shifts in the isotopic composition of seawater sulphate across the Permo-Triassic boundary in northern Italy.

Earth and Planetary Science Letters 218, 331-345.

Nielsen J. K., Shen Y., 2004. Evidence for sulfidic deep water during the late Permian in the East Greenland Basin. Geology 32, 1037–1040.

Nielsen J. K., Shen Y., Piasecki, S., Stemmerik, L., 2010. No abrupt change in redox condition caused the end-Permian marine ecosystem collapse in the East Greenland Basin. Earth and Planetary Science Letters 291, 32–38.

Nowlan, G.S., Barnes, C.R., 1987. Application of conodont colour alteration indices to regional and economic geology. In: Austin, R.L. (Ed.) *Conodonts: Investigative Techniques and Applications.* British Micropalaeontological Society Series, Ellis Horwood Limited, Chichester, 188–202.

Orchard, M. J., 2007. Conodont diversity and evolution through the latest Permian and Early Triassic upheavals. Palaeogeography, Palaeoclimatology, Palaeoecology 252, 93–117.

Orchard, M. J., 2010. Triassic conodonts and their role in stage boundary definition. In: Lucas, S. G. (Ed.) *The Triassic Timescale*. Geological Society of London Special Publication 334, 139–161.

Orchard, M.J., Krystyn, L., 2007. Conodonts from the Induan-Olenekian boundary interval at Mud, Spiti. *Albertiana* 35, 30-34.

Orchard, M.J., Tozer, E.T., 1997. Triassic conodont biochronology and intercalibration with the Canadian ammonoid sequence. *Albertiana* 20, 33-44.

Ovtcharova, M., Bucher, H., Schaltegger, U., Galfetti, T., Brayard, A., Guex, J., 2006. New Early to Middle Triassic U–Pb ages from South China: calibration with ammonoid biochronozones and implications for the timing of the Triassic biotic recovery. Earth and Planetary Science Letters 243, 463–475.

Payne, J.L., Lehrmann, D.J., Wei, J., Orchard, M.J., Schrag, D.P., Knoll, A.H., 2004. Large perturbations of the carbon cycle during recovery from the end-Permian extinction.

Science 305, 506–509.

Posenato, R., 2008. Global correlations of mid Early Triassic events: The Induan/Olenekian boundary in the Dolomites (Italy). Earth-Science Reviews 91, 93–105.

Purcell, R., 2006. Palynology Report Senecio-1, L1, North Perth Basin, Western Australia. Report to Arc Energy NL, 7pp.

Pruss, S.B., Bottcher, D.J., 2005. The reorganization of reef communities following the end-Permian mass extinction. Comptes Rendus Palevol 4, 553–568.

Retallack, G.J., Krull, E.S., 1999. Landscape ecological shift at the Permian–Triassic boundary in Antarctica. Australian Journal of Earth Sciences 46, 785–812.

Retallack, G.J., Veevers, J.J., Morante, R., 1996. Global coal gap between Permian–Triassic extinction and Middle Triassic recovery of peat-forming plants, Geol. Soc. Amer. Bull. 108, 195–207.

Richoz, S. Krystyn, L., Horacek, M., Spötl, C., 2007. Carbon isotope record of the Induan – Olenekian candididate GSSP Mud and comparison with other sections. Albertiana 35, 35-39.

Schubert, J.K., Bottjer, D.J., 1995. Aftermath of the Permian-Triassic mass extinction event: Paleoecology of Lower Triassic carbonates in the western USA. Palaeogeography, Palaeoclimatology, Palaeoecology 116, 1-39.

Sheldon, N.D., 2006. Abrupt chemical weathering increase across the Permian–Triassic boundary. Palaeogeography, Palaeoclimatology, Palaeoecology 231, 315– 321.

Shen, S.-Z., Henderson, C.M., Bowring, S.A., Cao, C.-Q., Wang, Y., Wang, W., Zhang, H., Zhang, Y.-C., Mu, L., 2010. High-resolution Lopingian (Late Permian) timescale of South China. Geological Journal 45, 122–134.

Shen, S.-Z., Crowley, J.L., Wang, Y., Bowring, S.A., Erwin, D.H., Sadler, P.M., Cao, C.-Q., Rothman, D.H., Henderson, C.M., Ramezani, J., Zhang, H., Shen, Y., Wang, X.-d.,

Wang, W., Mu, L., Li, W.-z., Tang, Y.-g., Liu, X.-l., Liu, L.-j., Jiang, Y.-f., Jin, Y.-g., 2011. Calibrating the end-Permian mass extinction. Science 334, 1367–1372.

Shigeta, Y., Zakharov, Y.D., Maeda, H., Popov, A.M., (Eds) 2009. *The Lower Triassic System in the Abrek Bay area, South Primorye, Russia.* Tokyo, National Museum of Nature and Science Monographs No. 38, 218pp.

Takahashi, S., Yamakita, S., Suzuki, N., Kaiho, K., Ehiro, M., 2009. High organic carbon content and a decrease in radiolarians at the end of the Permian in a newly discovered continuous pelagic section: A coincidence?, Palaeogeography, Palaeoclimatology, Palaeoecology 271, 1-12.

Thomas B. M., Barber C. J., 2004. A re-evaluation of the hydrocarbon habitat of the northern Perth Basin. Australian Petroleum Production & Exploration Association Journal 44, 59 – 92.

Thomas B. M., Willink R. J., Grice K., Twitchett R. J., Purcell R. R., Archbold N. W., George A. D., Tye S., Alexander R., Foster C. B., Barber C. J., 2004. Unique marine Permian – Triassic boundary section from Western Australia. Australian Journal of Earth Sciences 51, 423 – 430.

Tong, J., Yin, Y., 2002. The Lower Triassic of South China. Journal of Asian Earth Sciences 20, 803-815.

Tong, J., Zhao, L., 2011. Lower Triassic and Induan-Olenekian Boundary in Chaohu, Anhui Province, South China. Acta Geologica Sinica 85, 399-407.

Tong, J., Zakharov, Y. D., Orchard, M. J., Yin, H., Hansen, H. J., 2004. Proposal of Chaohu section as the GSSP candidate of the I/O boundary. Albertiana 29, 13-28.

Twitchett, R.J., 1999. Palaeoenvironments and faunal recovery after the end-Permian mass extinction. Palaeogeography, Palaeoclimatology, Palaeoecology 154, 27–37.

Twitchett, R.J., Wignall, P.B., 1996. Trace fossils and the aftermath of the Permo–Triassic

mass extinction: evidence from northern Italy. Palaeogeography, Palaeoclimatology, Palaeoecology 124, 137–151.

Wignall, P.B., Bond, D.P.G., Kuwahara, K., Kakuwa, Y., Newton, R.J., Poulton, S.W., 2010. An 80 million year oceanic redox history from Permian to Jurassic pelagic sediments of the Mino-Tamba terrane, SW Japan, and the origin of four mass extinctions. Global and Planetary Change 71, 109–123.

Wignall, P.B., Hallam, A., 1992. Anoxia as a cause of the Permian/Triassic extinction: Facies evidence from northern Italy and the western United States. Palaeogeography, Palaeoclimatology, Palaeoecology 93, 21–46.

Wignall, P.B., Hallam, A., 1993. Griesbachian (Earliest Triassic) palaeoenvironmental changes in the Salt Range, Pakistan and southeast China and their bearing on the Permo-Triassic mass extinction. Palaeogeography, Palaeoclimatology, Palaeoecology 102, 215 237.

Wignall, P.B., Newton, R., 2003. Contrasting Deep-water Records from the Upper Permian and Lower Triassic of South Tibet and British Columbia: Evidence for a Diachronous Mass Extinction. PALAIOS 18, 153–167.

Wignall, P.B., Newton, R., Brookfield, M.E., 2005. Pyrite framboid evidence for oxygen-poor deposition during the Permian–Triassic crisis in Kashmir. Palaeogeography, Palaeoclimatology, Palaeoecology 216, 183-188.

Wignall P. B., Twitchett R. J., 1996. Oceanic anoxia and the end-Permian mass extinction. Science 272, 1155–1158.

Wignall, P.B., Twitchett, R.J., 2002. Extent, duration and nature of the Permian-Triassic superanoxic event. In: Koeberl, C., MacLeod, K.C. (Eds) Catastrophic Events and Mass Extinctions: Impacts and Beyond. Boulder, Colorado. Geological Society of America Special Paper 356, 395-413.

Winguth, A.M.E, Maier-Reimer, E., 2005. Causes of the marine productivity and oxygen changes associated with the Permian–Triassic boundary: A reevaluation with ocean general circulation models. Marine Geology 217, 283-304.

Wignuth, C., Winguth, A.M.E, 2012. Simulating Permian–Triassic oceanic anoxia distribution: Implications for species extinction and recovery. Geology 40, 127–130.

Zhao L., Orchard M.J., Tong J., Sun, Z., Zuo, J., Zhang, S., Yun, A., 2007. Lower Triassic conodont sequence in Chaohu, Anhui Province, China and its global correlation. Palaeogeography, Palaeoclimatology, Palaeoecology 252, 24–38.

Zhao, L., Tong, J., Sun, Z., Orchard, M.J., 2008. A detailed Lower Triassic conodont biostratigraphy and its implications for the GSSP candidate of the Induan–Olenekian boundary in Chaohu, Anhui Province. Progress in Natural Science 18, 79–90.

Figure and Table Captions

Fig. 1. A. Location of Perth Basin and Senecio-1. B. End-Permian (253 Ma) palaeogeography showing locations of Senecio-1 and proposed GGSP sections at Chaohu and Mud. C. Upper Permian-Lower Triassic stratigraphy of the northern Perth Basin penetrated by Senecio-1, stratigraphic coverage of the cored interval shown in black. D. Generalised Permian-Triassic stratigraphy of the onshore Northern Perth Basin (after Mory et al., 2005).

Fig. 2. Organic metamorphic facies and maturity indices showing the maturity level indicated for the Senecio-1 sediments based on conodont and spore color. Partly after Metcalfe and Riley (2010), Nowlan and Barnes (1987) and Epstein, Epstein and Harris (1977).

Fig. 3. *Clarkina* spp. Pa elements, all sample C36 (2716.75-2717.00 m depth), Senecio-1 core. 1,2. Oral and inner lateral views of specimen C36/1. 3,4. Oral and inner lateral views of specimen C36/2. 5,6. Oral and inner lateral views of specimen C36/3. 7,8. Oral and inner lateral views of specimen C36/4.

Fig 4. *Neospathodus dieneri* Sweet Pa elements, Senecio-1 core. 1. Specimen C29/5, lateral view, sample C29 (2715.00-2715.25 m depth). 2. Specimen C29/8, lateral view, sample C29 (2715.00-2715.25 m depth). 3. Specimen C49/3, lateral view, sample C49 (2720.00-2720.25 m depth). 4. Specimen C53/16, lateral view, sample C53 (2721.00-2721.25 m depth). 5. Specimen C76/1, lateral view, sampleC76 (2726.75-2727.00 m depth). 6-14 all from sample C77 (2727.00-2727.25 m depth): 6. Specimen C77/23, lateral view; 7,8. Oral and outer lateral views of specimen C77/1; 9, 10. Oral and inner

lateral views of specimen C77/2; 11. Lateral view of specimen C77f; 12, 13. Lateral and oral views of specimen C77/11; 14. Lateral view of specimen C77d.

Fig. 5. *Neospathodus novaehollandiae* McTavish Pa elements, Senecio-1 core. 1,2,3,4. Oral, oblique oral, inner lateral and outer lateral views of specimen C29/3, sample C29 (2715.00-2715.25 m depth). 5. Inner lateral view of specimen C25/7. sample C25 (2714.00-2714.25 m depth). 6. Inner lateral view of Holotype specimen number UWA69120B of McTavish (1973) reimaged using the SEM for comparison with Senecio-1 material.

Fig. 6. *Neospathodus pakistanensis* Sweet Pa elements, Senecio-1 core. 1. Lateral view of specimen C10/1, sample C10 (2710.25-2710.50 m depth). 2, 3. Oral and inner lateral views of specimen C25/3, sample C25 (2714.00-2714.25 m depth). 4, 5. Lateral and basal views of specimen C25/2, sample C25 (2714.00-2714.25 m depth). 6. Lateral view of specimen C25/8, sample C25 (2714.00-2714.25 m depth). 7. Lateral view of specimen C29/4, sample C29 (2715.00-2715.25 m depth). 8. Lateral view of specimen C10/16, C10 (2710.25-2710.50 m depth).

Fig. 7. *Neospathodus waageni eowaageni* Zhao & Orchard Pa elements, Senecio-1 core. 1. Lateral view of specimen C25/26, sample C25 (2714.00-2714.25 m depth). 2. Lateral view of specimen C35/7, sample C35 (2716.50-2716.75 m depth).

Fig. 8. *Neospathodus waageni waageni* Sweet Pa elements, Senecio-1 core, from sample C28 (2714.75-2715.00 m depth). 1,2,3. Oral, outer lateral and anterior views of specimen C28/2. 4, 5. Oral and inner lateral views of specimen C28/3. 6-9. Oral, anterior, outer

lateral and posterior views of specimen C28/4.

Fig. 9. *Neospathodus waageni* subsp. nov. A Pa elements, Senecio-1 core. 1. Lateral view of specimen C20/1, sample C20 (2712.75-2713.00 m depth). 2. Lateral view of specimen C20/5, sample C20 (2712.75-2713.00 m depth). 3. Lateral view of specimen C23/8, sample C23 (2713.50-2713.75 m depth). 4. Lateral view of specimen C20/2, sample C20 (2712.75-2713.00 m depth). 5. Lateral view of specimen C23/4, sample C23 (2713.50-2713.75 m depth). 6. Lateral view of specimen C25/1, sample C25 (2714.00-2714.25 m depth). 7. Lateral view of specimen C20/3, sample C20 (2712.75-2713.00 m depth). 8. Lateral view of specimen C23/6, sample C23 (2713.50-2713.75 m depth). 9. Lateral view of specimen C28/5, sample C28 (2714.75-2715.00 m depth).

Fig. 10. Ranges of important conodont taxa and conodont zones, ocurrence of pelagic macro-fossils and bioturbation index values in the Senecio-1 core and placement of the Induan-Olenekian boundary.

Fig. 11. Correlation of the $\delta^{13}C$ curve and conodont zones for Senecio-1 core with those of proposed Induan-Olenekian GSSP sections at Chaohu, China and Mud, India.

Fig. 12. Temporal and geographic distribution of deep and shallow-marine dysoxia and anoxia in the Late Permian and early Triassic plotted against physical, biotic and chemostratigraphic events that relate to the late Changhsingian mass extinction and 5 million year long Early Triassic cesspool. Permian-Triassic numerical timescale is compiled from Mundil et al. (2004), Ovtcharova et al. (2006), Lehrmann et al. (2006), Galfetti et al. (2007b), Mundil et al. (2010), Shen et al. (2010) and Shen et al. (2011).

Carbon isotope curve (adjusted to the latest numerical timescale) and gastropod size data are from Payne et al. (2004). Shallow-marine temperature curve from Joachimski et al. (2012). Chemical weathering intensity from Algeo et al. (2011). Reef frameworks, unusual facies and radiolarian data from Knoll et al. (2007), Pruss and Bottcher (2005) and Brayard et al., (2011). Coal seam thickness data from Retallack et al. (1996). Sources of temporal distribution of dysoxia and anoxia are discussed in the text.

Table 1. Senecio-1 Carbon isotope samples, total organic carbon (wt%) and δ13C values.

Figure 1

Click here to download high resolution image

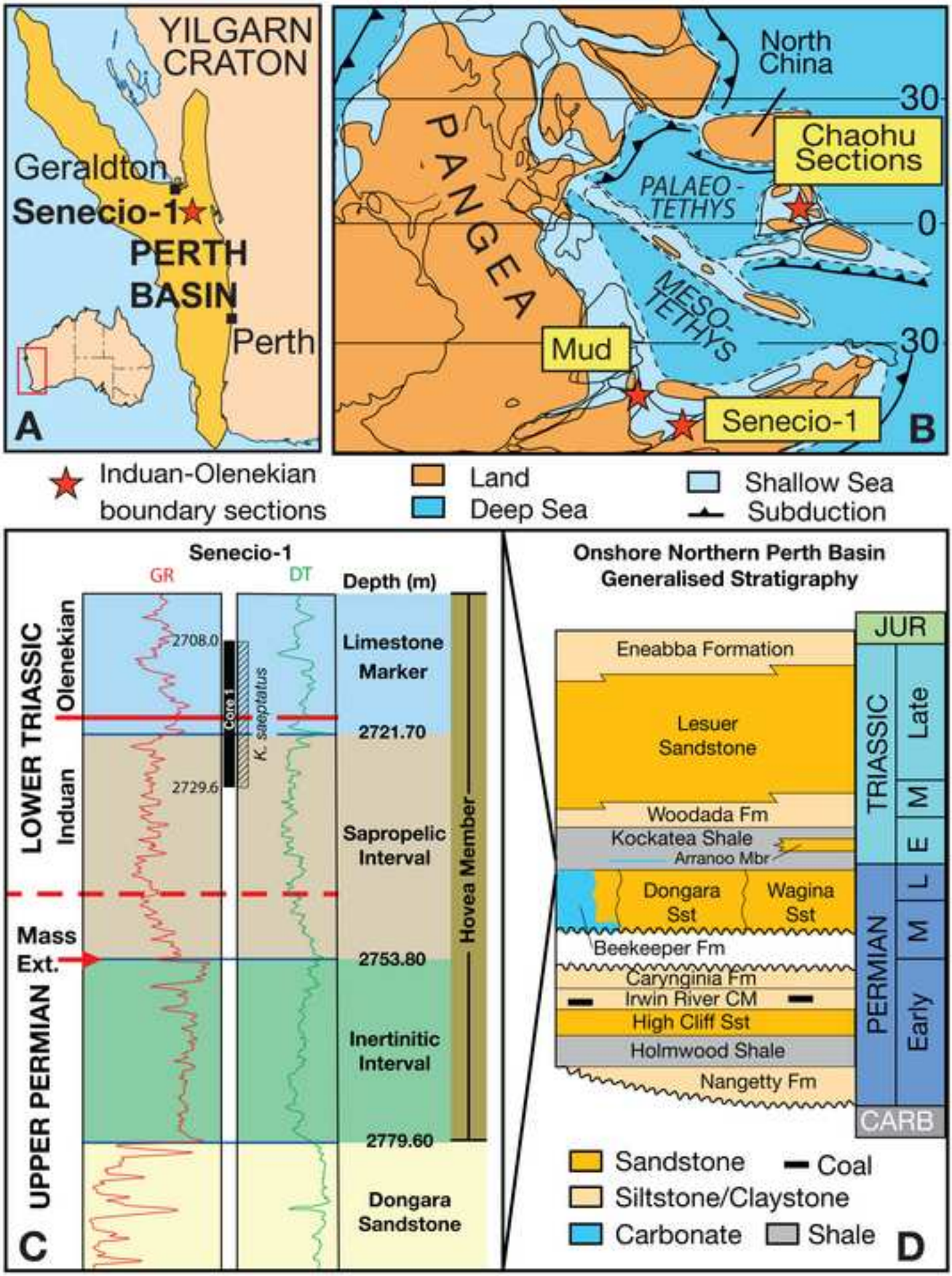

Figure 2

Click here to download high resolution image

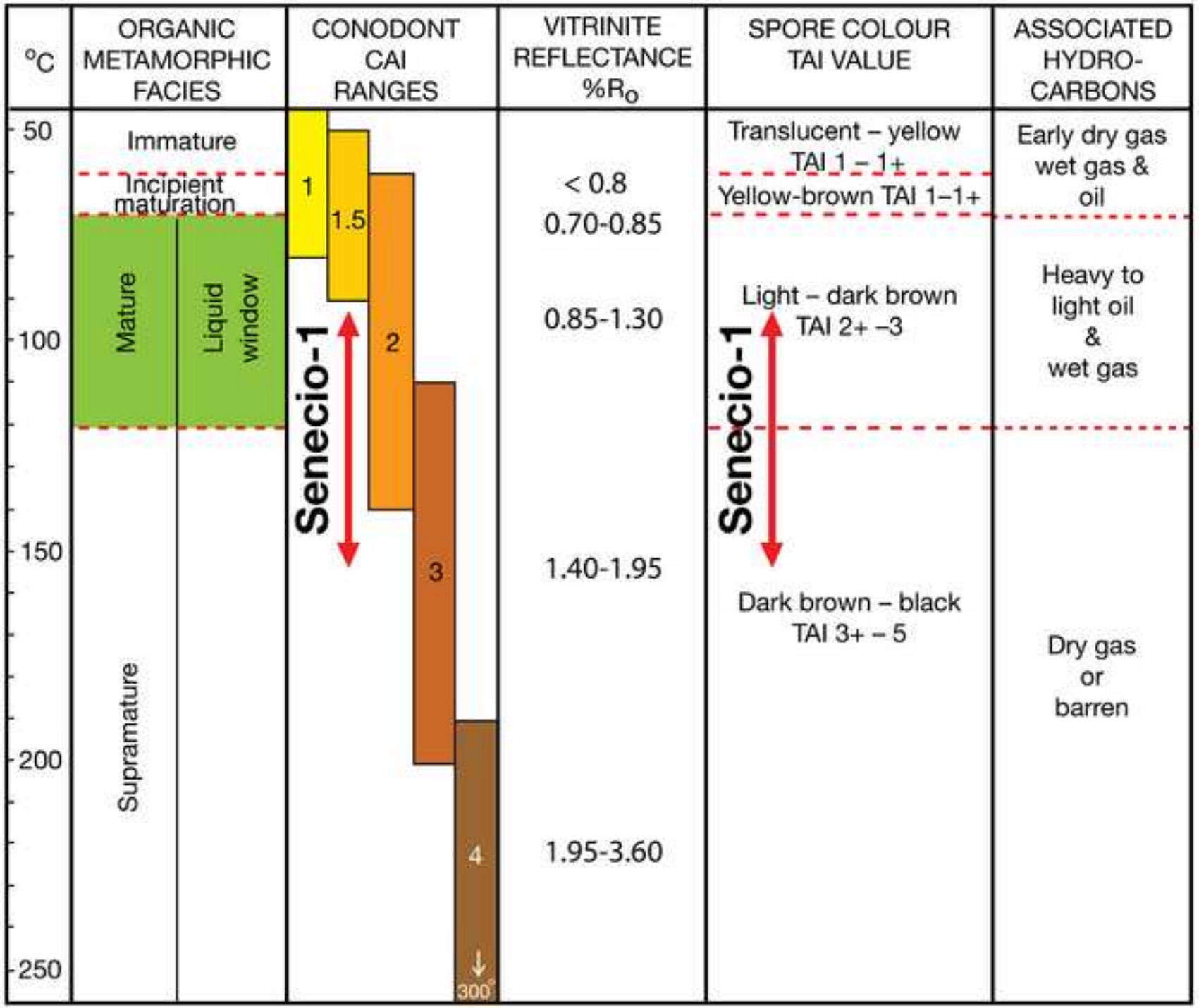

Figure 3

Click here to download high resolution image

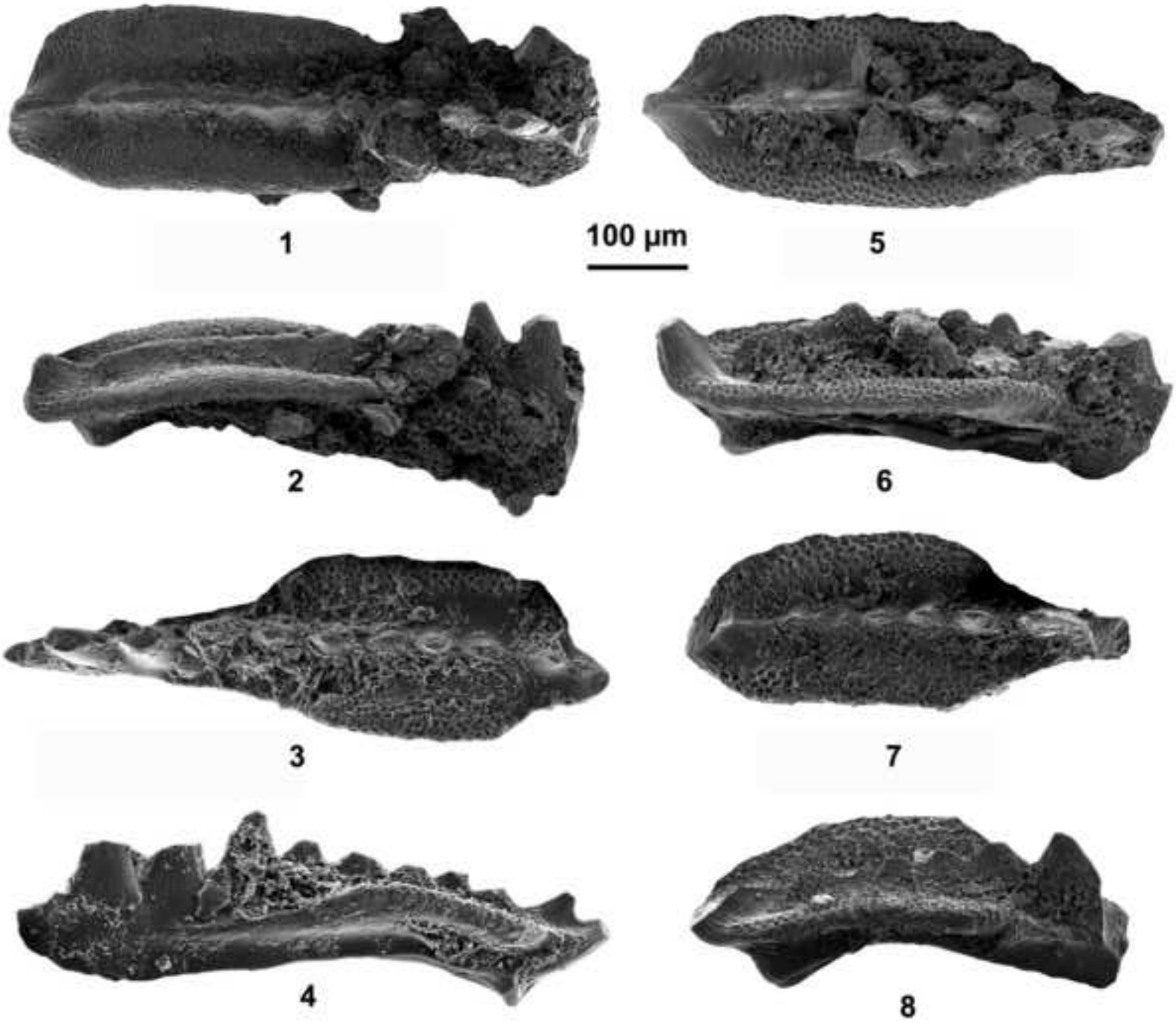

Figure 4

Click here to download high resolution image

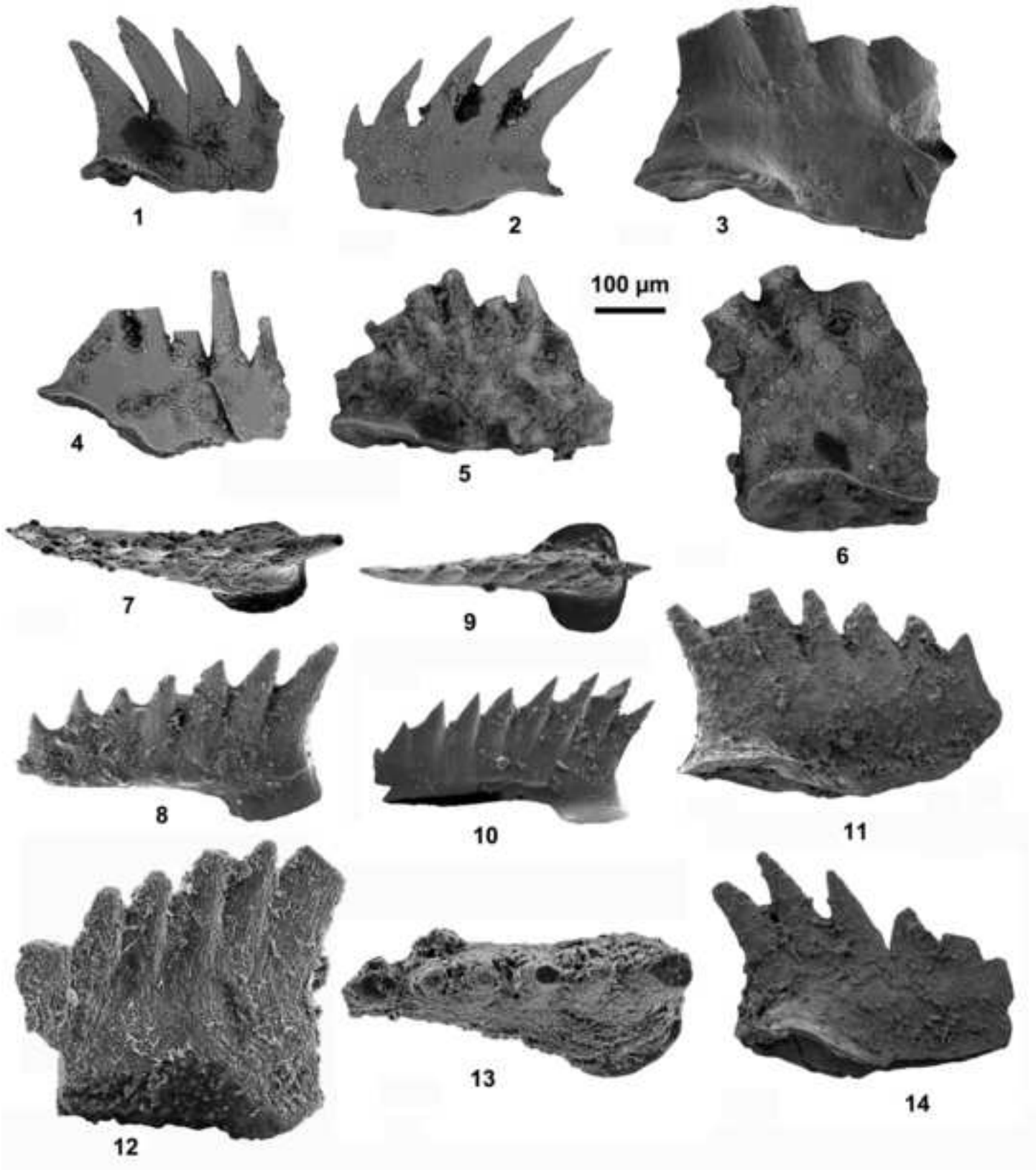

Figure 5

Click here to download high resolution image

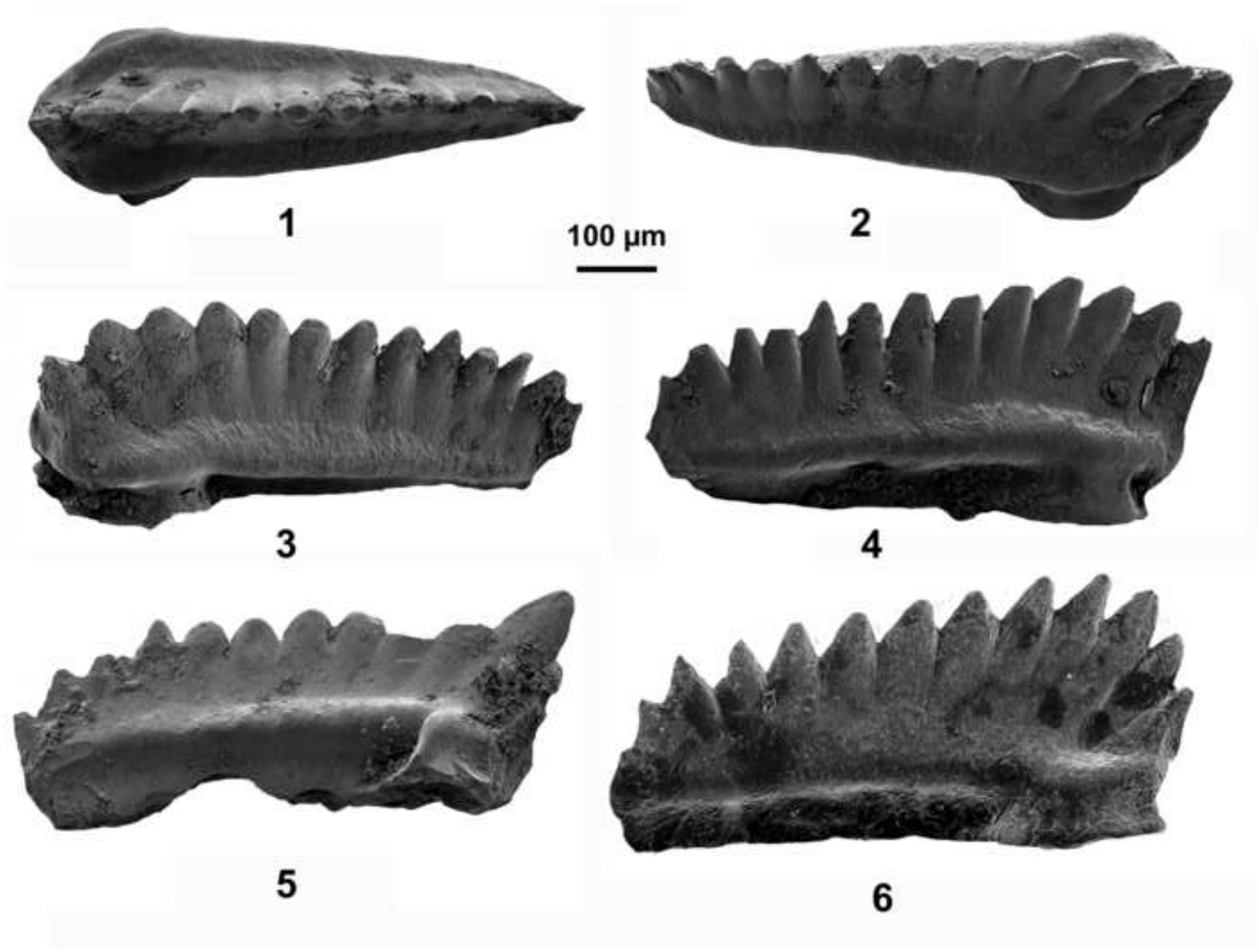

Figure 6

Click here to download high resolution image

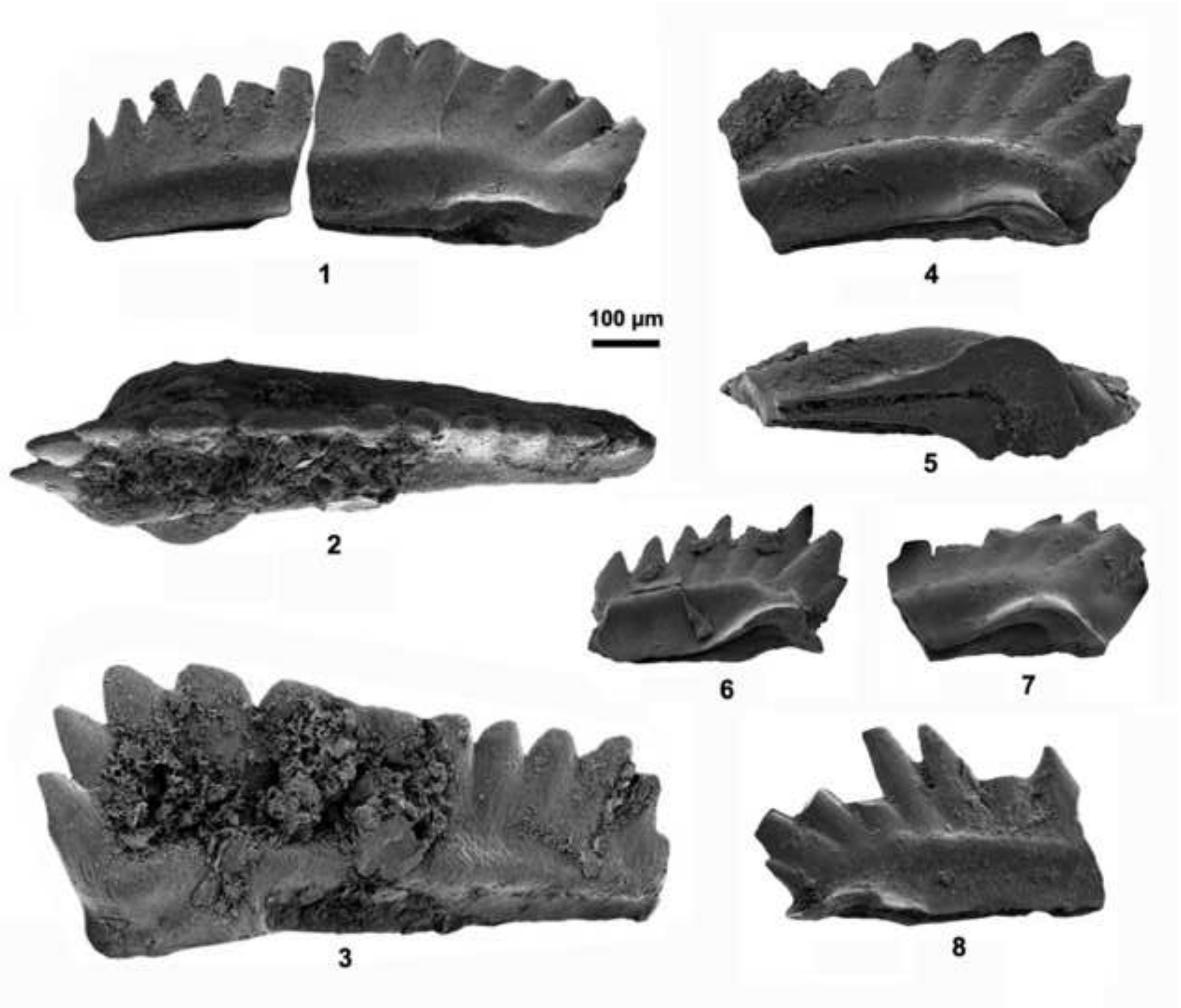

Figure 7

Click here to download high resolution image

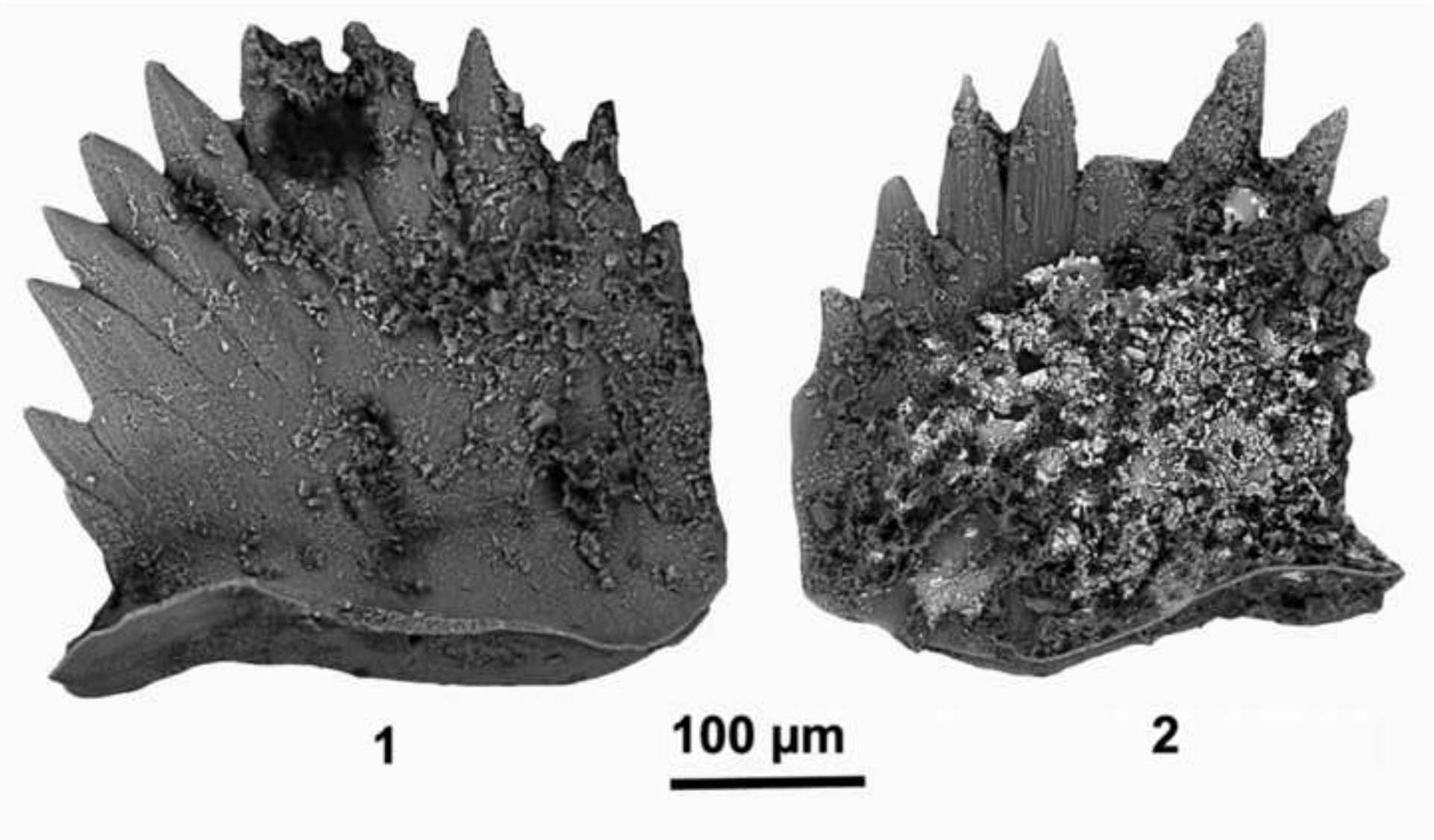

Figure 8

Click here to download high resolution image

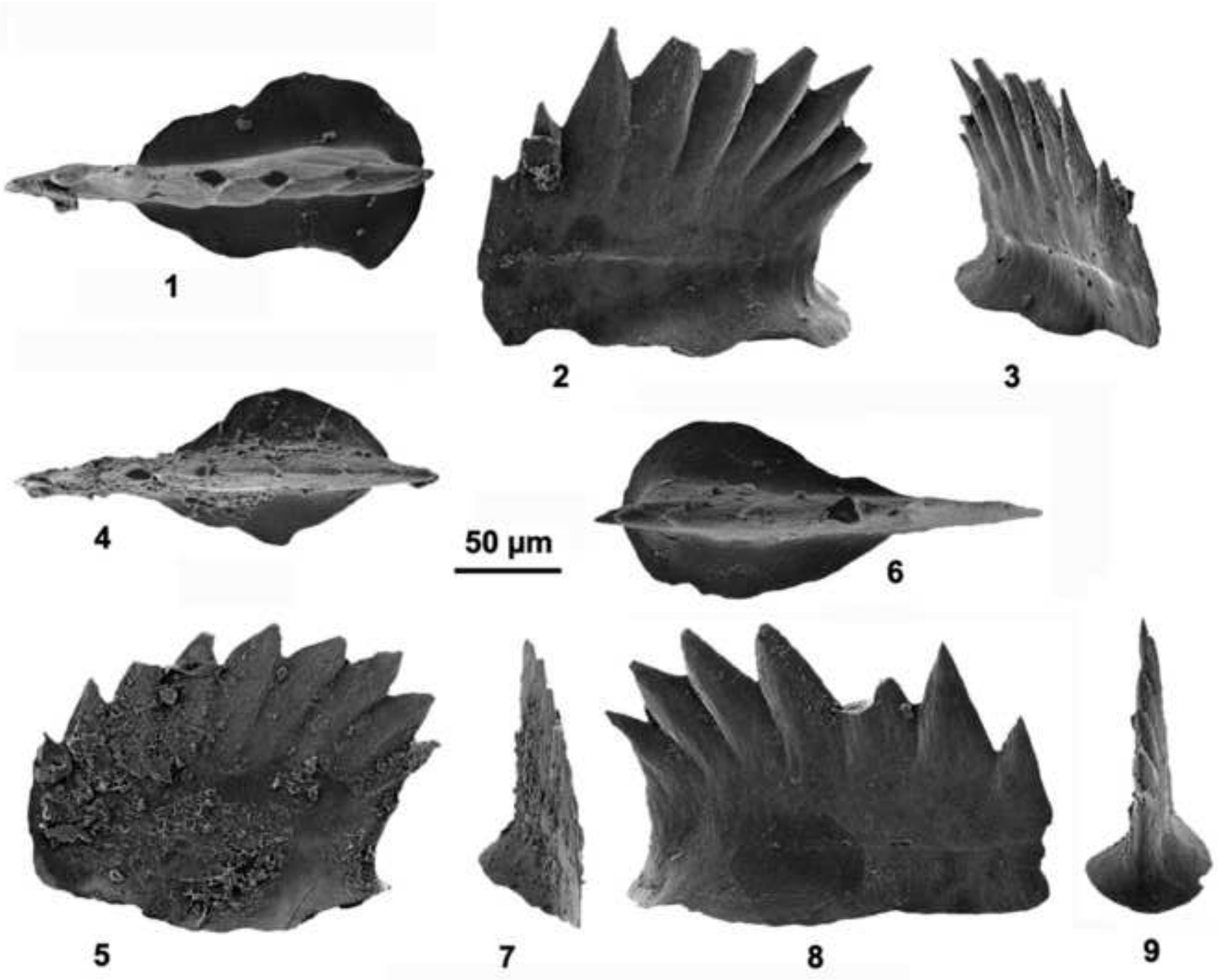

Figure 9

Click here to download high resolution image

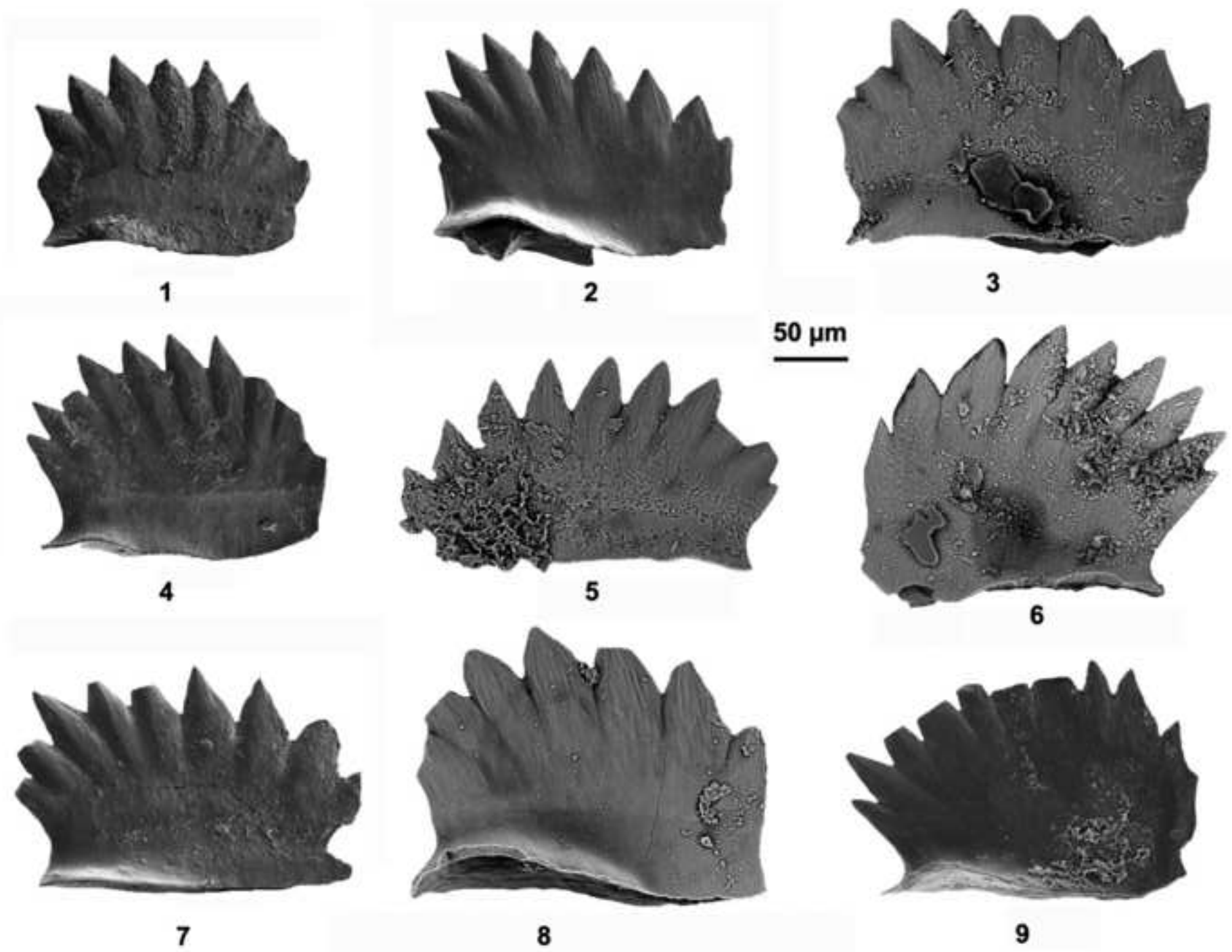

Figure 10

Click here to download high resolution image

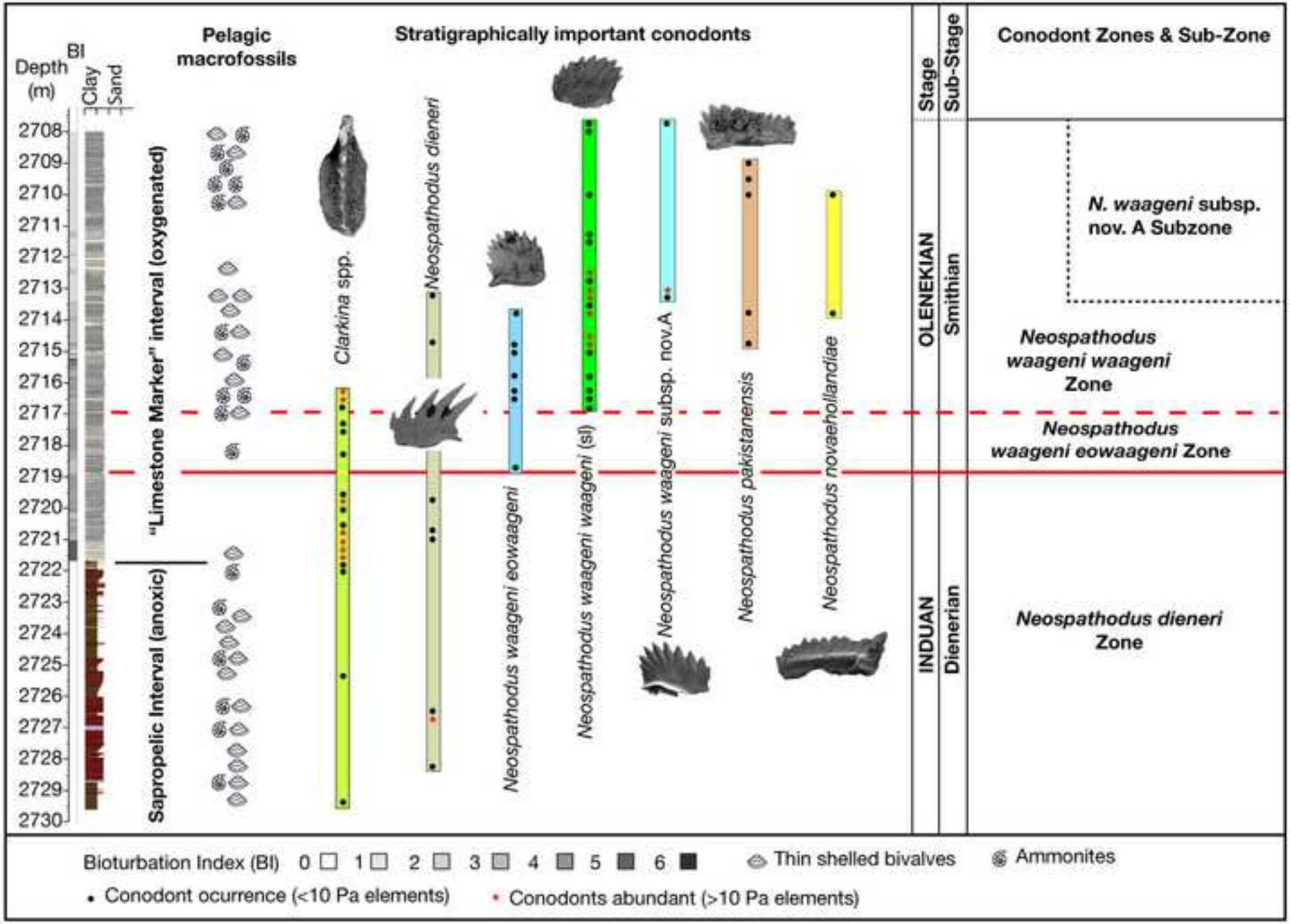

Figure 11

Click here to download high resolution image

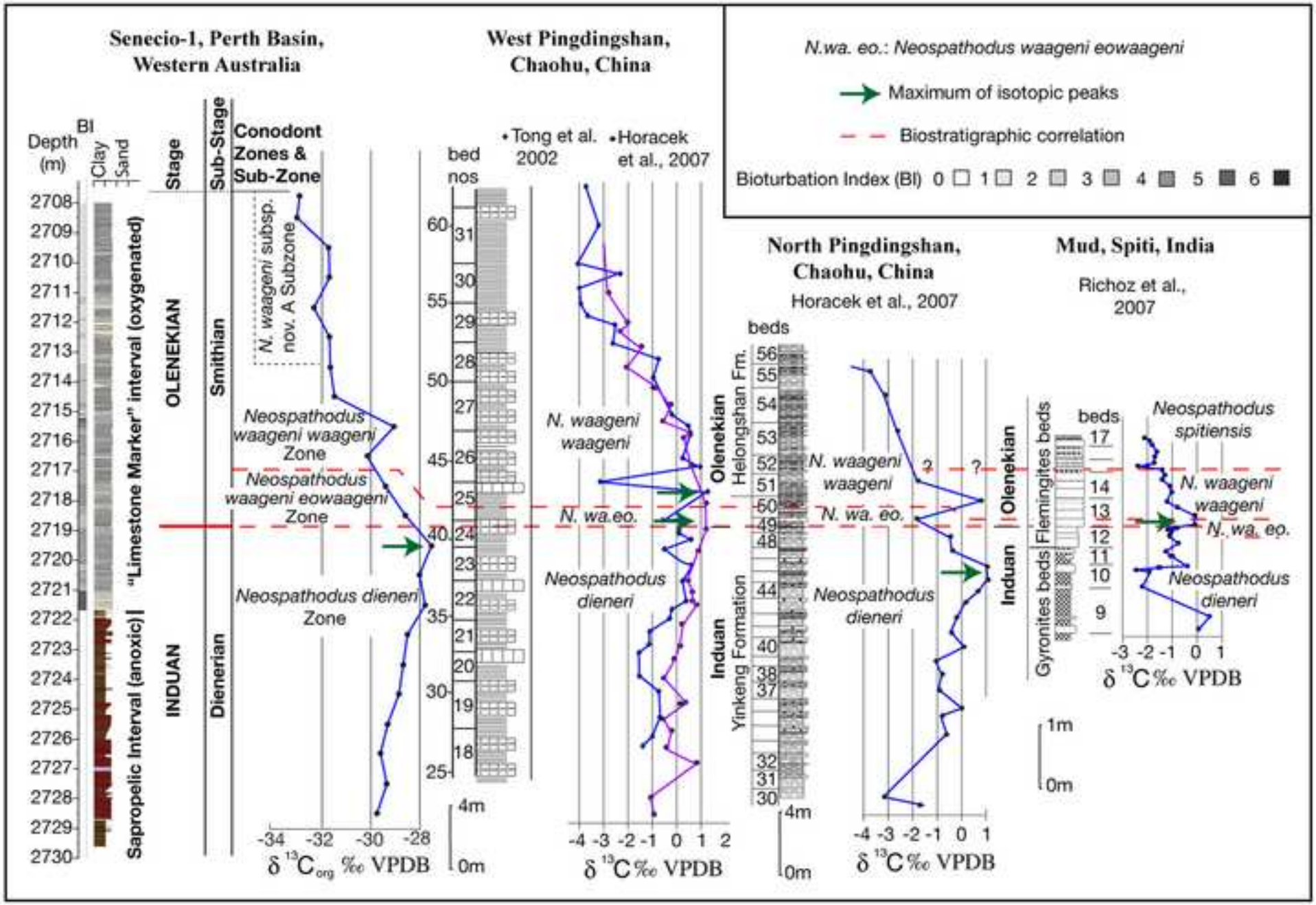

Figure 12

Click here to download high resolution image

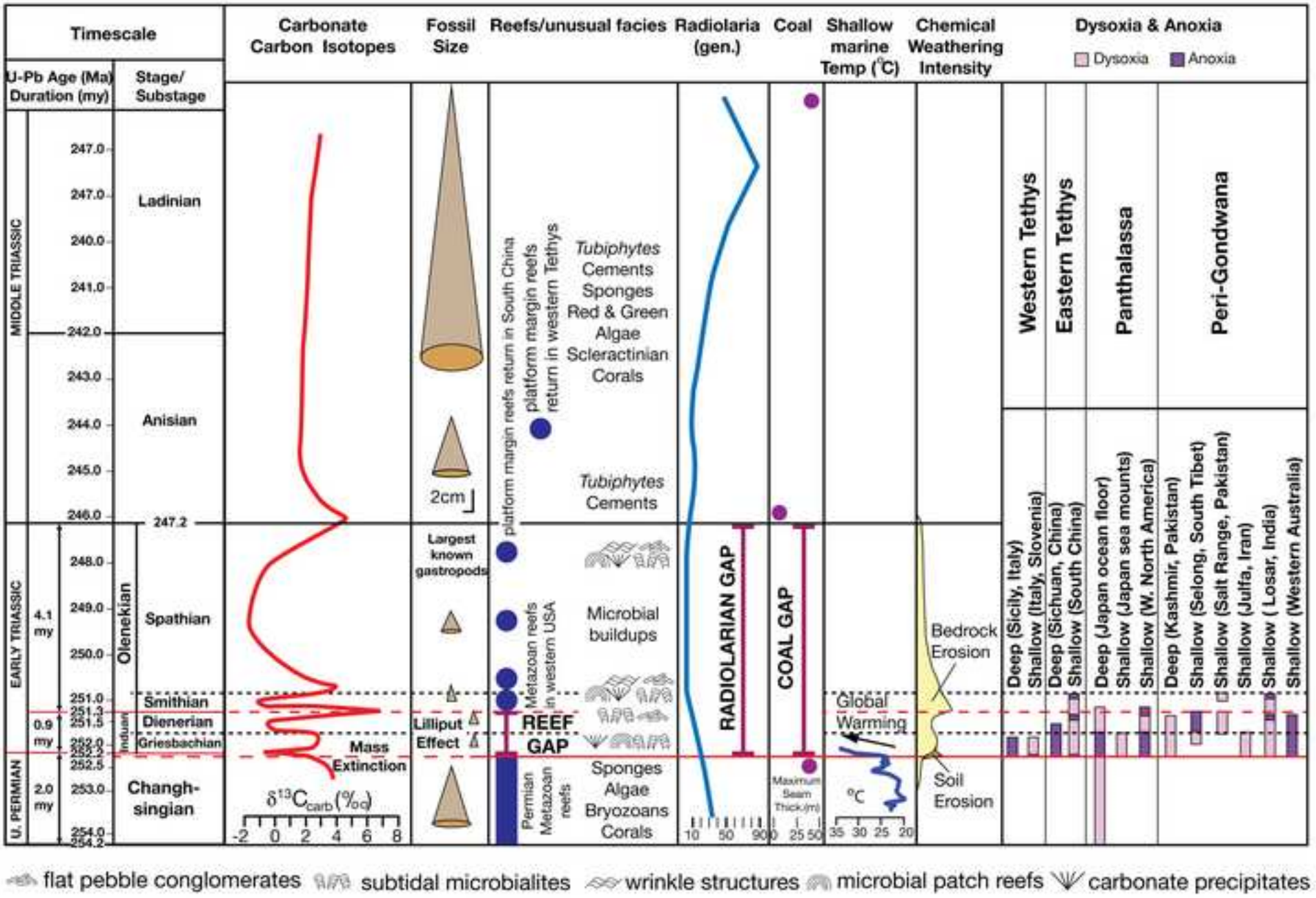

Table 1

Table 1. Senecio-1 Carbon isotope samples, total organic carbon (wt%) and δ13C values.

Sample no.	Depth (m)	C [wt%]	δ13C [‰ VPDB]
1	2708.10 - 2708.14	0.4	-32.88
4	2708.85 - 2708.87	0.5	-32.91
8	2709.83 - 2709.86	0.3	-31.8
12	2710.84 - 2710.87	0.2	-31.82
16	2711.92 - 2711.95	0.4	-32.3
20	2712.88 - 2712.91	0.4	-31.79
24	2713.82 - 2713.83	0.3	-31.69
28	2714.88 - 2714.90	0.4	-31.54
32	2715.85 - 2715.87	0.6	-28.98
36	2716.81 - 2716.84	0.4	-30.18
40	2717.90 - 2717.92	0.7	-29.44
44	2718.92 - 2718.95	0.4	-28.61
48b	2719.85 - 2719.88	0.3	-27.52
52	2720.87 - 2720.89	0.5	-28.03
56	2721.94 - 2721.96	1.4	-27.9
60	2722.91 - 2722.93	1.2	-28.5
64	2723.85 - 2723.87	0.9	-28.79
68	2724.88 - 2724.90	1.7	-28.95
72	2725.88 - 2725.90	1	-29.31
76	2726.88 - 2726.91	1.5	-29.66
80	2727.85 - 2727.88	2	-29.37
84	2728.85 - 2728.88	1.4	-29.89

Research Highlights

- Induan-Olenkian boundary identified using conodonts in the Perth Basin, Australia
- $\delta^{13}C_{org}$ positive excursion peak correlates with Induan-Olenekian boundary globally
- Early Triassic dysoxia/anoxia linked to environmental perturbations and upwelling

*Graphical Abstract (for review)